AD-A086 263 CALIFORNIA UNIV LOS ANGELES DEPT OF MATERIALS F/6 20/11
ACOUSTIC EMISSION ARISING FROM PLASTIC DEFORMATION AND FRACTURE--ETC(U)
MAY 80 K ONO N00014-75-C-0419
UNCLASSIFIED TR-80-02 NL

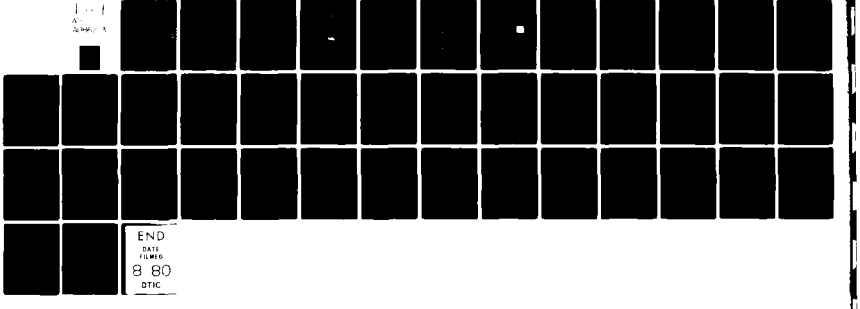

END
DATE FILMED
8 80
DTIC

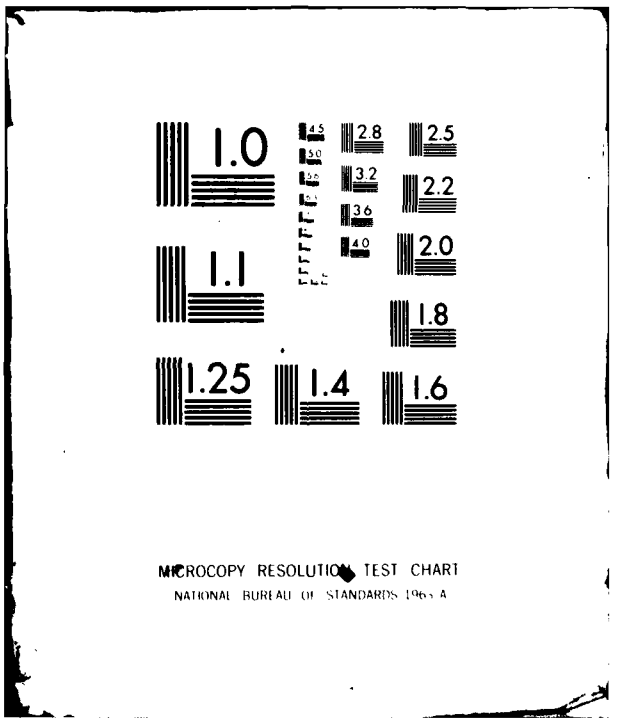
1.0
1.1
1.25
1.4
1.6
1.8
2.0
2.2
2.5
2.8
3.2
3.6
4.0
4.5
5.0
MICROCOPY RESOLUTION TEST CHART
NATIONAL BUREAU OF STANDARDS 1963 A

(12) LEVEL II

SECURITY CLASSIFICATION OF THIS PAGE (When Data Entered)

REPORT DOCUMENTATION PAGE

READ INSTRUCTIONS BEFORE COMPLETING FORM

1. REPORT NUMBER: ONR Technical Report No. 80-02	2. GOVT ACCESSION NO.: AD-A086263
3. RECIPIENT'S CATALOG NUMBER:	
4. TITLE (and Subtitle): Acoustic Emission arising from Plastic Deformation and Fracture.	5. TYPE OF REPORT & PERIOD COVERED: Technical rept.
	6. PERFORMING ORG. REPORT NUMBER:
7. AUTHOR(s): Kanji Ono	8. CONTRACT OR GRANT NUMBER(s): N00014-75-C-0419
9. PERFORMING ORGANIZATION NAME AND ADDRESS: Materials Department, 6531-Boelter Hall, University of California, Los Angeles, CA 90024	10. PROGRAM ELEMENT, PROJECT, TASK AREA & WORK UNIT NUMBERS:
11. CONTROLLING OFFICE NAME AND ADDRESS: Physics Program, ONR-800 North Quincy Street, Arlington, Virginia 22217	12. REPORT DATE: May 1980 13. NUMBER OF PAGES: 41
14. MONITORING AGENCY NAME & ADDRESS (if different from Controlling Office): 42	15. SECURITY CLASS. (of this report): Unclassified 15a. DECLASSIFICATION DOWNGRADING SCHEDULE:

16. DISTRIBUTION STATEMENT (of this Report)

Unlimited

DISTRIBUTION STATEMENT A
Approved for public release;
Distribution Unlimited

DTIC ELECTE JUN 27 1980 S D B

17. DISTRIBUTION STATEMENT (of the abstract entered in Block 20, if different from Report)

(14) TR-80-02

18. SUPPLEMENTARY NOTES

Presented at the special session on Acoustic Emission during the Joint Meeting of ASA and ASJ, December 1, 1978, Honolulu, Hawaii and was published in its Proceedings volume entitled "Fundamentals of Acoustic Emission."

19. KEY WORDS (Continue on reverse side if necessary and identify by block number)

Acoustic Emission
Generation and detection
Acoustic Emission Theory
Plastic Deformation
Fracture

20. ABSTRACT (Continue on reverse side if necessary and identify by block number)

see the next page

406237 Jm

DD FORM 1 JAN 73 1473 EDITION OF 1 NOV 65 IS OBSOLETE
S/N 0102 LF 014 6601

SECURITY CLASSIFICATION OF THIS PAGE (When Data Entered)

80 6 24 017

7

ACOUSTIC EMISSION ARISING FROM PLASTIC DEFORMATION AND FRACTURE

Kanji Ono

Materials Department
School of Engineering and Applied Science
University of California, Los Angeles, CA

ABSTRACT

This paper reviews current status of acoustic emission signal detection methods, theoretical analysis of acoustic emission sources and acoustic emission behavior of materials arising from plastic deformation and fracture. Recent developments in quantitative signal detection and transducer characterization are considered. Several theories of acoustic emission sources are summarized and one based on dislocation theory by Málen and Bolin is extended to provide a relation between the inelastic displacement at a source to the peak voltage output of a resonant transducer. Models of acoustic emission from plastic deformation are presented. A new model for continuous acoustic emission is developed on the basis of the modified Malén-Bolin theory. Predictions of the model are discussed in conjunction with recent studies on acoustic emission behavior as a function of test temperature and of heat treatment. Finally, acoustic emission due to cracking is evaluated, especially in relation to amplitude distribution analysis of burst-type emission.

I. INTRODUCTION

Research and developmental efforts in acoustic emission (AE) have been rapidly growing in recent years. AE methods have firmly established their usefulness as a tool for nondestructive evaluation, as many encouraging results of successful applications have been reported. Numerous studies have been presented in this Volume characterizing AE behavior of various materials and components and linking it to underlying causes of emission. However, much work still remains to be done in both basic and applied aspects of AE. In order to identify the advances in the basic aspect of AE, we will review recent accomplishments of various investigations, concentrating on AE signal detection and analysis techniques. For those interested in earlier developments, the reviews and conference proceedings listed at the end should prove valuable[1-15]. Because of time limitation, many areas of AE research have not been touched upon in this review. Some of the papers presented in this Volume should provide excellent starting points for seeking information in these areas.

II. SIGNAL DETECTION

2.1 Introduction

While there have been a number of studies to develop models of surface motion in the field of seismology (see e.g. Knopoff[16]), the first quantitative attempt to analyze AE signals was made by Breckenridge et al.[17]. The main purpose of such an attempt is to deduce the characteristics of the source of AE signals, from which it is hoped to discriminate different types of AE signals. The AE signals observed in a practical system are influenced by the characteristics of a piezoelectric transducer and those of wave propagation through the structure (including its resonance characteristics). Consequently, as we pointed out earlier[18], the analysis in the frequency domain has not been effective in the characterization of AE sources. However, apparently different frequency (or power density) spectra have been extracted from various types of AE signals[18-23]. The main sources of such findings appear to originate from the mode of excitation of transducer and structural (specimen) resonances. Theoretical analysis of the excitation modes is so complex that it would be difficult to factor out the resonating effects of the transducer and the wave transmission characteristics. From a practical point of view, however, frequency spectrum analysis ought not to be discounted. While empirical information must be accumulated for a particular application, a unique combination of transducer excitation and wave transmission characteristics can provide a useful tool for the identification (or classification) of AE sources.

2.2 Quantitative Measurements

Let us now consider the AE generation and detection systems, in which every aspect has been well-characterized. One such system was developed at the National Bureau of Standards (NBS) by Breckenridge et al[17]. Quantitative AE source characterization at NBS has since been continued and expanded[24]. An important element of their contributions is the development of mechanical source simulators. The first one employed a short section of glass capillary, having a diameter of about 0.1 mm, which was fractured under compressive loading. The statically applied force was released upon fracture with a rise time of less than 0.1 μs. The fracture process of the capillary has, however, a large variability in the magnitude of the force step. Thus, the second simulator has become a preferred technique[24]. Here, a pencil lead is used as the fracturing element. A common mechanical pencil is mounted on a jig to break a fixed length of the lead. The rise time of the force step produced by this method was measured to be 0.3 μs. The amplitude and the waveform of the resultant stress pulse have been found to be quite consistent. It is useful in applications as well. One such simulator was employed to determine wave propagation and attenuation characteristics of a fiber-composite pressure vessel[25].

As for the detector of stress wave, the NBS group used an air-gap capacitance transducer[17,24]. It was used to convert a surface displacement to a proportional electrical signal. Another group active in this area is located at U.K. Atomic Energy Research Establishment, Harwell[26-28]. The Harwell group, led by Scruby and Wadley, developed a refined capacitance transducer using a differential micrometer which allowed the adjustment of the air-gap for constant sensitivity (Fig. 1)[27]. The sensitivity of the transducer to surface displacement u_s, is given by

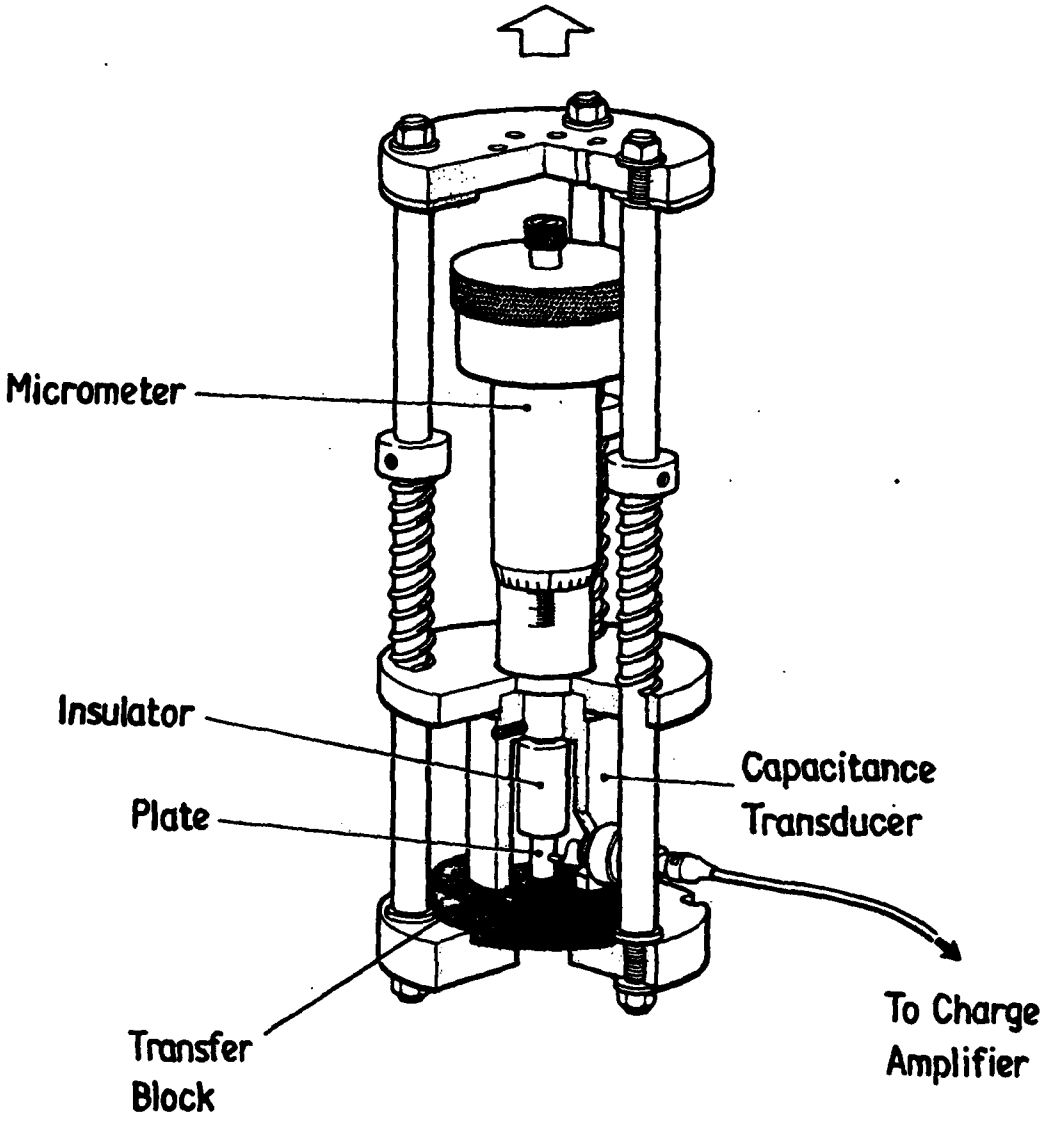

Figure 1. Cutaway drawing of capacitance transducer, showing the differential micrometer used to adjust the plate separation.[27]

$$\frac{dq}{du_s} = -\frac{\varepsilon_o V A_t}{g^2} \qquad (2.1)$$

where q is a charge, ε_o is the dielectric constant of an air gap, g is the distance of the air gap, V is the potential difference and A_t is the area of the capacitance transducer respectively. Thus, the sensitivity increases by increasing V and A_t and decreasing g. Limitations on V and g are imposed by electrical discharge and by surface finishes. A_t must also be limited to avoid averaging of non-planar wavefront. The air-gap was typically 5 μm and the voltage across capacitor plates was 50 V. In combination with a charge sensitive pre-amplifier, they obtained the sensitivity of the order of 1 pm (10^{-12} m) and the rise time resolution of 20 ns. The latter limit was imposed by the amplification and signal recording, as well as the size of the capacitor plate (6 mm diameter).

Another important element of an AE system is the medium of wave propagation. The NBS group used large plates of steel, glass and aluminum to model the elastic wholespace and halfspace, for which theoretical solutions for the wave propagation characteristics are available. Two propagation paths have been studied. In the first, wave propagated on the surface from the point where a force step was applied. At a distance r, the primary (P or longitudinal) wave arrives first, followed by the secondary (S or shear) and Rayleigh (R) waves. Vertical displacement reaches a maximum at the arrival of R wave[16,29,30]. The second path was through the elastic medium and vertical displacement was measured exactly above the point source; this is referred to as the epicenter, borrowed from the seismology. When a plate is used to simulate the elastic halfspace, only the initial part of the displacement-time curve is a valid representation. However, this arrangement has initially proven to be satisfactory. In response to a force step at a depth H, vertical displacement on the surface at the epicenter shows a jump upon the arrival of the P wave. The magnitude of this jump u_p, was given by [28,30]

$$u_p = 0.047\ (\Delta F/\mu H)\ u(t - H/c_L), \qquad (2.2)$$

where ΔF is the force step, μ is the shear modulus, t is time and c_L is the longitudinal wave velocity and u(t) is a unit step (Heaviside) function, respectively. Here, the numerical constant was calculated using the wave velocities for steel. Note that i(t) = 1 for t > 0 and u(t) for t 0. The jump is followed by a gradual rise to the arrival of the S wave (Fig. 2). In both of these experiments, the observed wavforms agree with theoretically predicted ones (Fig. 3). More recently, a theoretical solution for an elastic plate was obtained and compared with an experimentally determined epicenter displacement record[24]. By scaling at a reference point, the two curves agreed quite well (Fig. 4). The theory can provide numerical solutions to other more complex cases, including a plate of limited size and different types of applied forces[24,31,32]. In the case of the epicenter displacement, the Harwell group obtained a quantitative agreement between theory and experiment[27]. Using the calibrated capacitance transducer, aluminum plates of different thicknesses and a pencil lead fracture source,

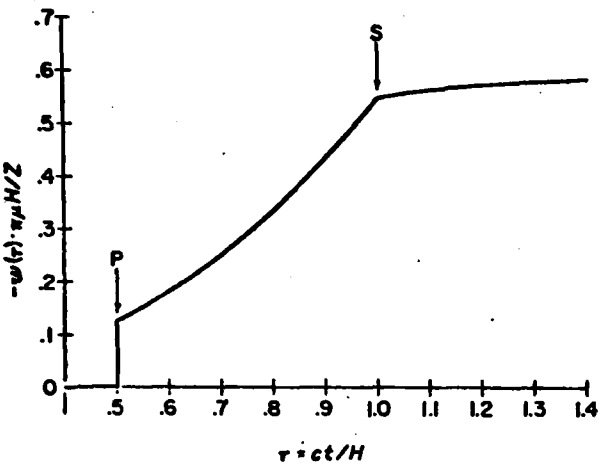

Figure 2. Vertical displacement for seismic buried pulse calculated from expressions of Pekeris and Lifson[30] for $\nu = 1/3$. P and S show the arrivals of the longitudinal and shear waves, respectively.[17]

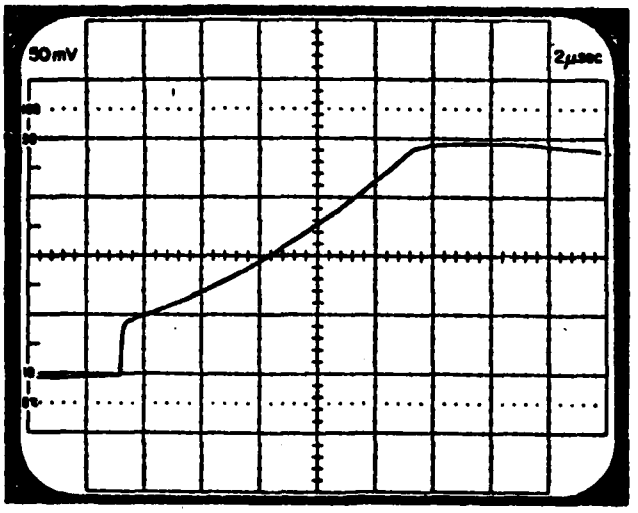

Figure 3. Oscillogram showing the vertical displacement at a point on one surface of a block resulting from a step of load applied to the other surface directly opposite.[17] The block is an aluminum-alloy block; source, breaking of glass capillary 0.1 mm in diameter; air gap, 4.1 μm; polarization, 200V. Each division on the abscissa equals 2 μs.

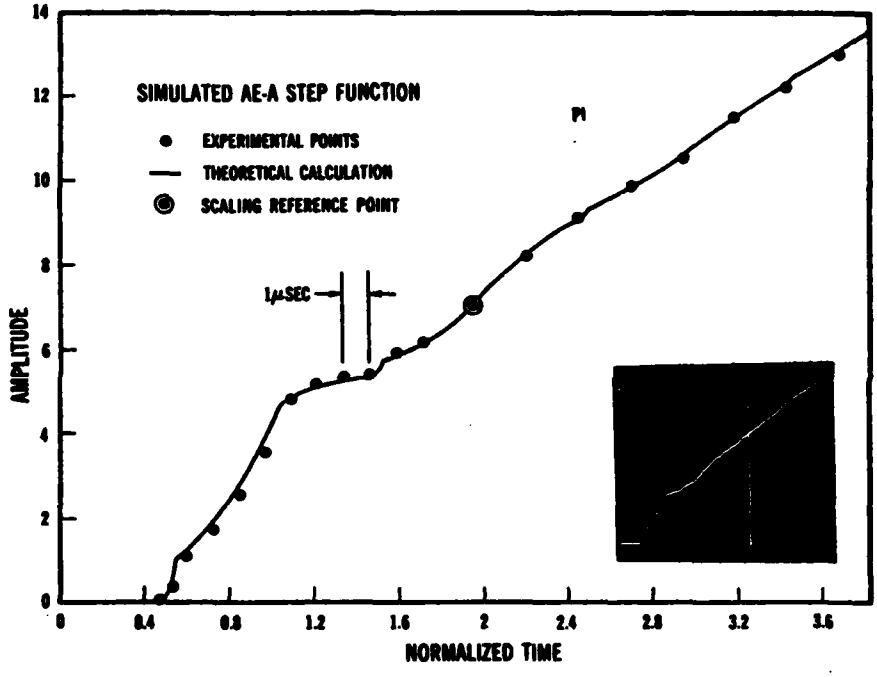

Figure 4. Comparison between theoretical calculation of the vertical displacement as computed by the generalized ray method and the experimentally measured voltage output of capacitive transducer at the epicenter of aluminum plate 23 cm x 44 cm x 2.52 cm.[24] The scaling reference point is where the experimental amplitude is set to equal the theortical amplitude.

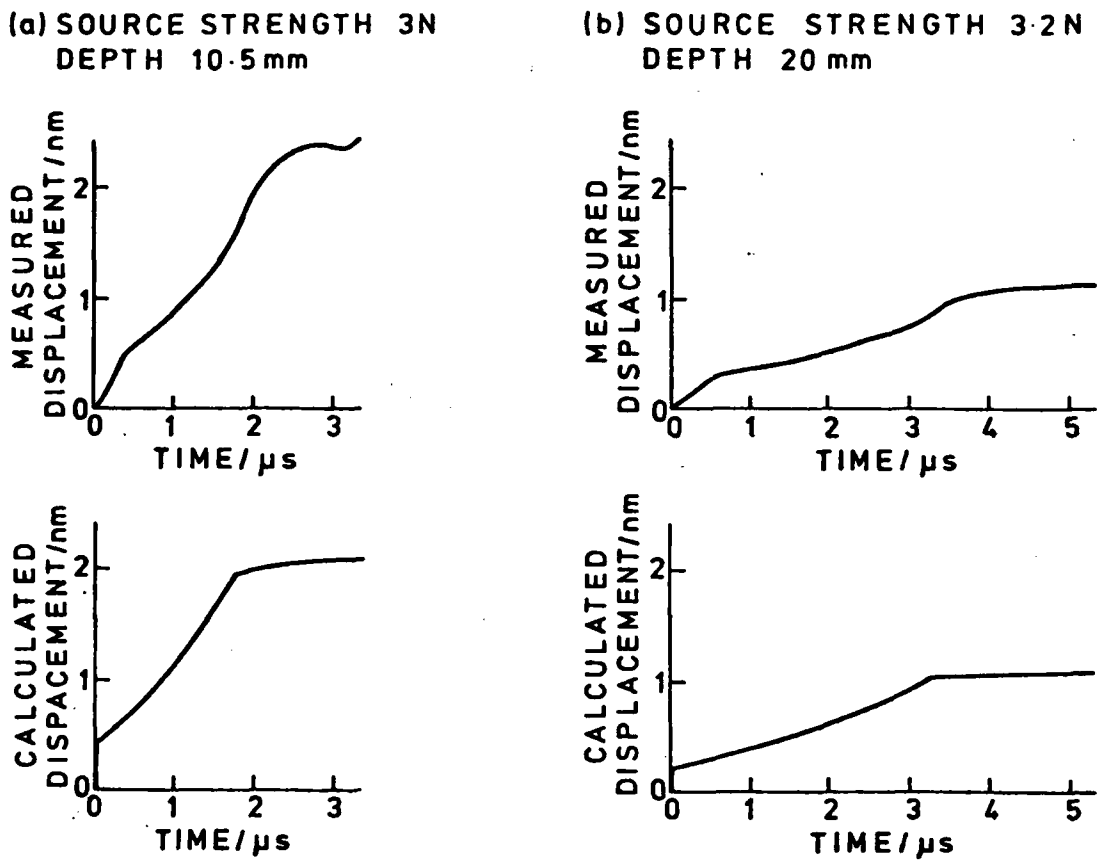

Figure 5. Surface displacement of two aluminium blocks of different thickness, in response to the fracture of a pencil lead vertically above the detector.[27] The experimental values were measured using the capacitance transducer and the calculated values were from a theoretical model based on Pekeris & Lifson.[30] The time is measured from the arrival of the longitudinal pulse.

they found the magnitude of displacements at the P and S arrivals to be in good accord with those calculated from a model of Pekeris and Lifson[30] (Fig. 5). The experimental waveforms, however, exhibit the effect of a finite rise time of the source. Here, the magnitude of a force step, the elastic moduli and the depth of source (plate thickness) were provided for the calculations.

2.3 Detection of Real AE Signals

Scruby and Wadley[26,28] conceived the most innovative experiment in the quantitative AE study. They invented a special specimen geometry, called Yobell (Fig. 6), which preserved the essential features of the elastic halfspace, yet allowing to perform the mechanical testing of materials. Using their calibrated capacitance transducer, Wadley and Scruby[26] captured the waveforms of AE signals due to microfracture events in EN30A steel (0.3% C, 3% Ni, 0.7% Cr). Burst-type AE signals during the fracture of quenched, and quenched-tempered (including temper embrittled conditions) specimens were analyzed for their rise time and amplitude. A typical one is shown in Fig. 7. Effects of hydrogen charging were also examined. They found that the rise time for the quenched samples to be 70-78 ns, which was reduced to 47-73 ns for temper embrittled conditions (see Table I)[26]. The former had the fracture mode of 45° shear with central undulating area, while the latter exhibited predominately cup and cone fracture with some isolated areas of brittle fracture. Additions of hydrogen increased intergranualr fracture and resulted in the increased rise time: 87 ns for the quenched and 75 to 131 ns for the temper embrittled. This distribution of measured rise time is given in Fig. 8. They interpret the rise time as the life time of an AE source and the amplitude to the area of a crack increment[26]. While a great deal more of study will be needed to quantitatively link the source event to observed signal characteristics, this work at Harwell certainly ranks as one of the most significant advances in AE research.

2.4 Transducer and System Calibration

The developments of well characterized AE systems also allow an improved description of a piezoelectric transducer of common usage. Reproducible generation of a displacement-time function enable the calibration of a transducer. The result for a commercially available transducer was reported[24], indicating its sensitivity to surface velocity rather than displacement, at least during the initial part of the transducer excitation. Figure 9 compares the output of a piezoelectric transducer and a displacement waveform. Because of significant effects due to the coupling layer, more studies are required to establish a standard calibration facility. In this regard, the availability of a calibrated displacement (capacitance) transducer allows one to produce a secondary calibration standard using a piezoelectric transducer coupled to a plate. For the calibration of actual AE measurement systems, however, simpler mechanical sources, such as pencil lead fracturing and helium gas jet devices[33], may still be advantageous in convenience.

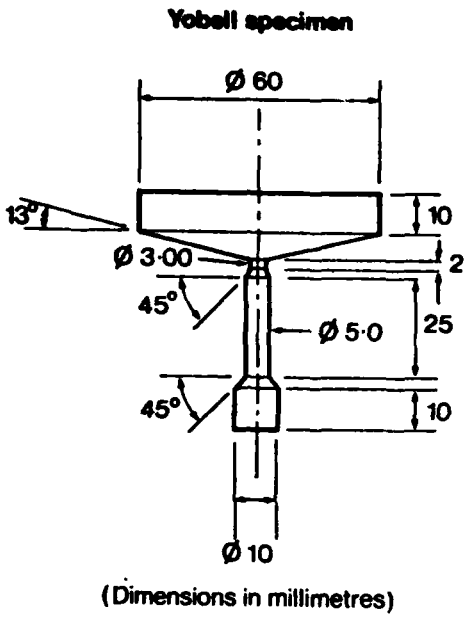

Figure 6. The geometry of Yobell specimen.[26]

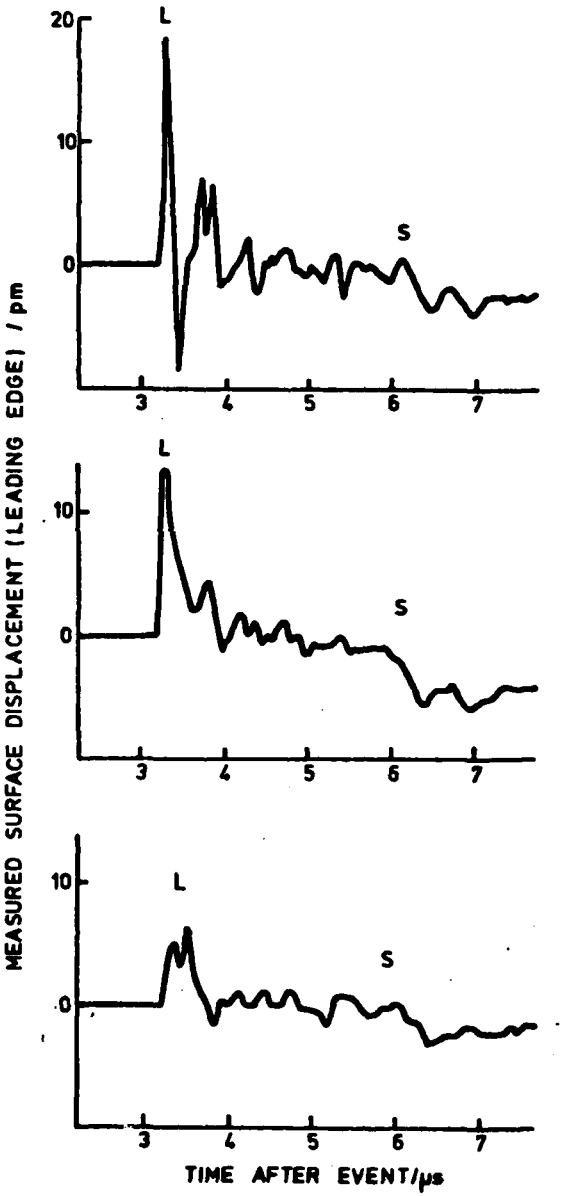

Figure 7. A typical transient measured with the calibrated broad band system.[26]

TABLE 1

Fracture Modes and Acoustic Emission Risetime Data

Specimen	Condition	Fracture Mode	No. Transients in dynamic range	Average Risetime/ns
D1	Quenched	45° shear with central undulating area	12	70
D2			5	72
D3			2	78
D4	Tempered	Cup and Cone	1	67
D5	Temper Embrittled	90% intergranular	11	76
D6		Predominantly ductily cup + cone isolated areas of brittle mode	13	57
D7			28	47
D8			24	63
D9			25	56
H1	Quenched	45° shear with central undulating area + 5% inter-granular	13	87
H2	Tempered	Cup and cone with ~5% intergranular	3	106
H3	Temper Embrittled	Intergranular + isolated areas of tearing	19	106
H4			10	75
H5			-	-
H6			3	131
H7			-	-
H8			-	-

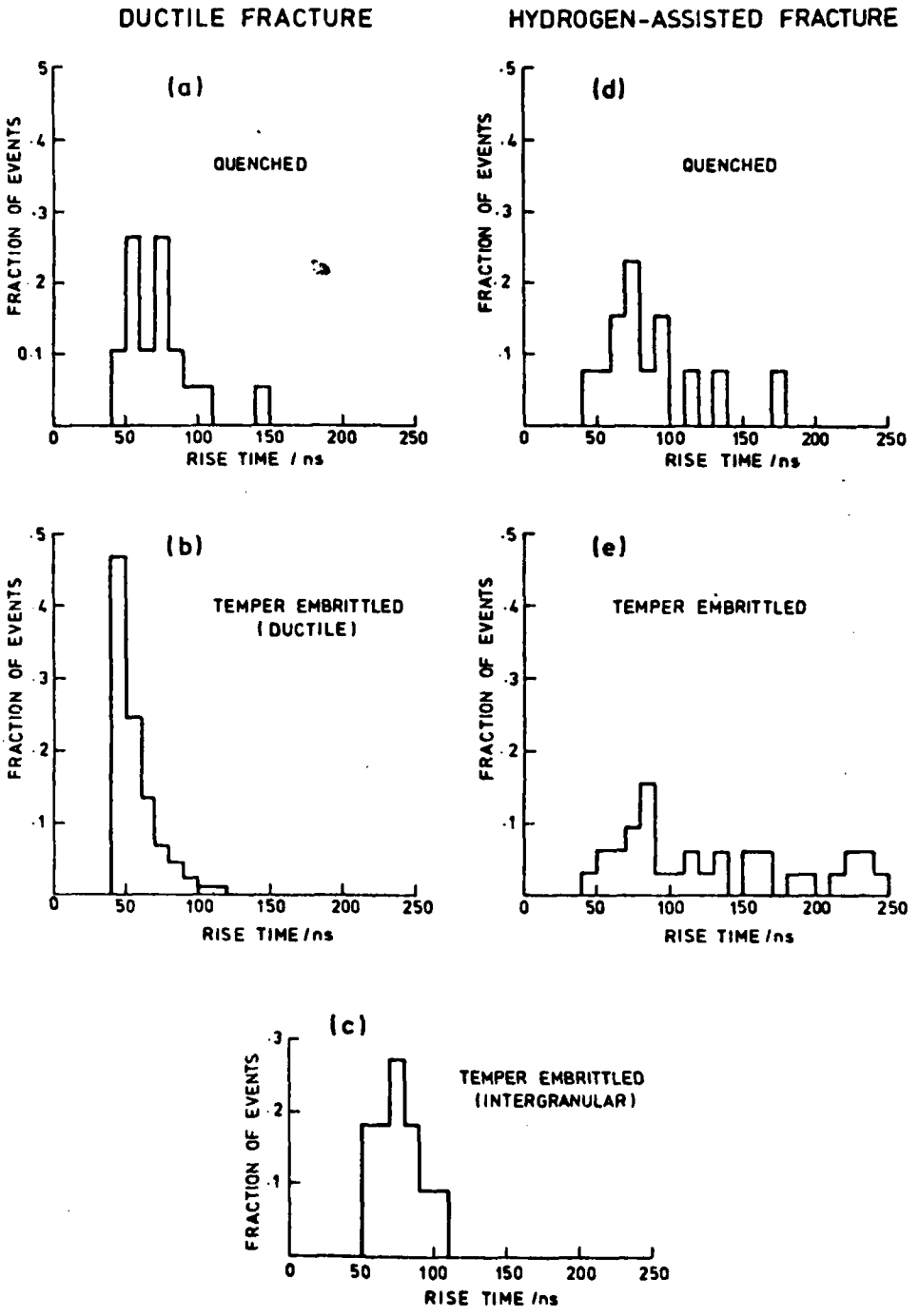

Figure 8. Rise time distributions of acoustic emission transients recorded during the fracture of EN 30A steel in different conditions.[26]

Hatano and Mori proposed another approach to transducer calibration based on reciprocity theorem[34]. In this scheme, a set of three transducers is arranged to form three pairs of transmitter-received combination, assuming that each transducer possesses reciprocal transmitting and receiving characteristics. By feeding tone bursts of variable frequency and recording the output voltages, sensitivity calibration to surface wave was accomplished. Using a large steel forging weighing 7 tons, Hatano[35] extended the technique to longitudinal wave calibration. Transducer coupling remains to be a source of uncertainty in this calibration method.

2.5 Other Transducers

Electromagnetic AE transducers have been used in monitoring of welds and other applications despite their low sensitivity (10 to 100 times less sensitive compared to piezoelectric transducers) and their vulnerability to electromagnetic interferences[36]. The primary advantage is the non-contact nature. Maxfield and Hulbert reviewed this subject[37].

Another approach is based on an optical principle, that is, laser interferometer, having a stabilized optical path difference (Fig. 10). For a bandwidth of 1 MHz, a minimum detectable displacement of 50 pm (5×10^{-11} m) was achieved. This limit was mostly due to the noise arising from the laser used. They demonstrated that AE signals from twinning, stress corrosion cracking and thermal shock cracking can be detected by the optical method. An example is shown in Fig. 11, in comparison to the waveform detected by a piezoelectric transducer. Taking advantage of non-contact nature, Blacic and Hagmann[39] reported another optical-mechanical system for AE measurements at high temperatures and pressure. Here, interferometer fringe motion was detected and converted, by quadrature logic, to a linear analog signal proportional to stress. Since optical techniques have inherently broad bandwidth and can be calibrated absolutely, these should compliment the well developed capacitance transducers for standardization and would be most valuable when the remote sensing characteristics are essential.

2.6 Waveform Analysis Techniques

When theoretical responses of a structure and the source and transducer characteristics are known, it is still necessary to perform mathematical operation, known as convolution, in order to obtain the resultant waveform. Conversely, deconvolution must be performed in order to obtain the source characteristic from the observed waveform, structural response function and transducer characteristics. It is generally necessary to resort to elaborate numerical computations. Such computations can be simplified in the frequency domain, since the convolution-deconvolution of a time function can be substituted in the frequency domain by the multiplication-division of the frequency. Houghton[40] attempted to develop a hardwired device to obtain the source characteristics and reported some success. The NBS troup has been investigating several different means of implementing a deconvolution scheme. Their

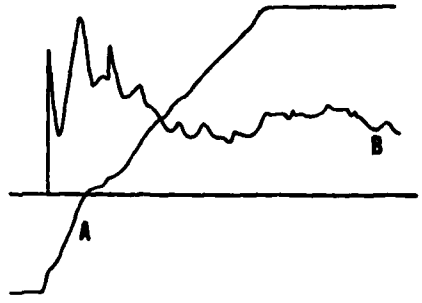

Figure 9. Comparision od detected signals (oscilloscope traces) with two different sensors: A is for the capacitive displacement transducer and B is for a piezoelectric transducer.[24] The duration of these traces is 40 μsec.

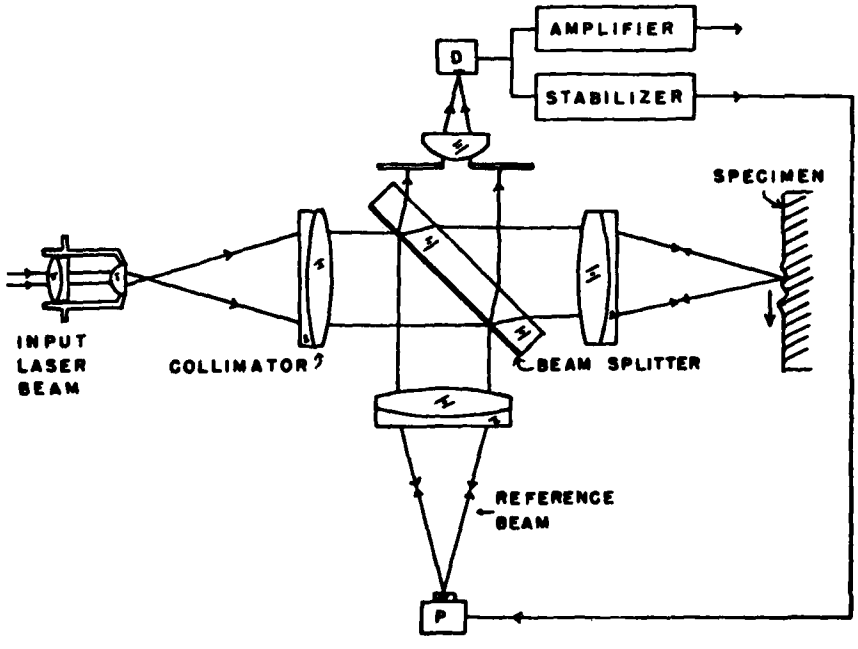

Figure 10. Stabilized optical path interferometer for measurement of acoustic emission signals.[38] Stabilized system removes low frequency (0-1 kHz) distrubances; the high frequency signals (>10 kHz) are amplified and recorded.

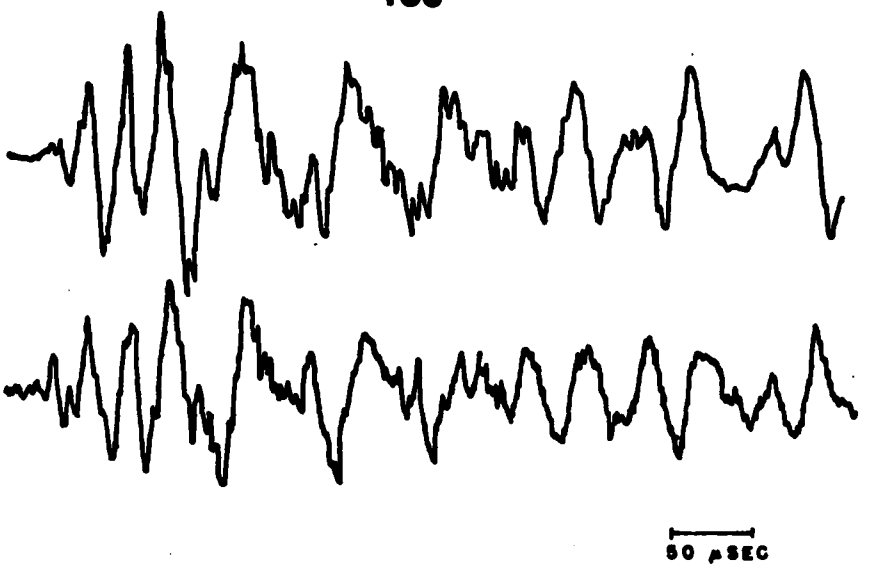

Figure 11. Acoustic emission signals due to single twin in zinc: upper trace piezoelectric signal; lower trace optical signal.[38]

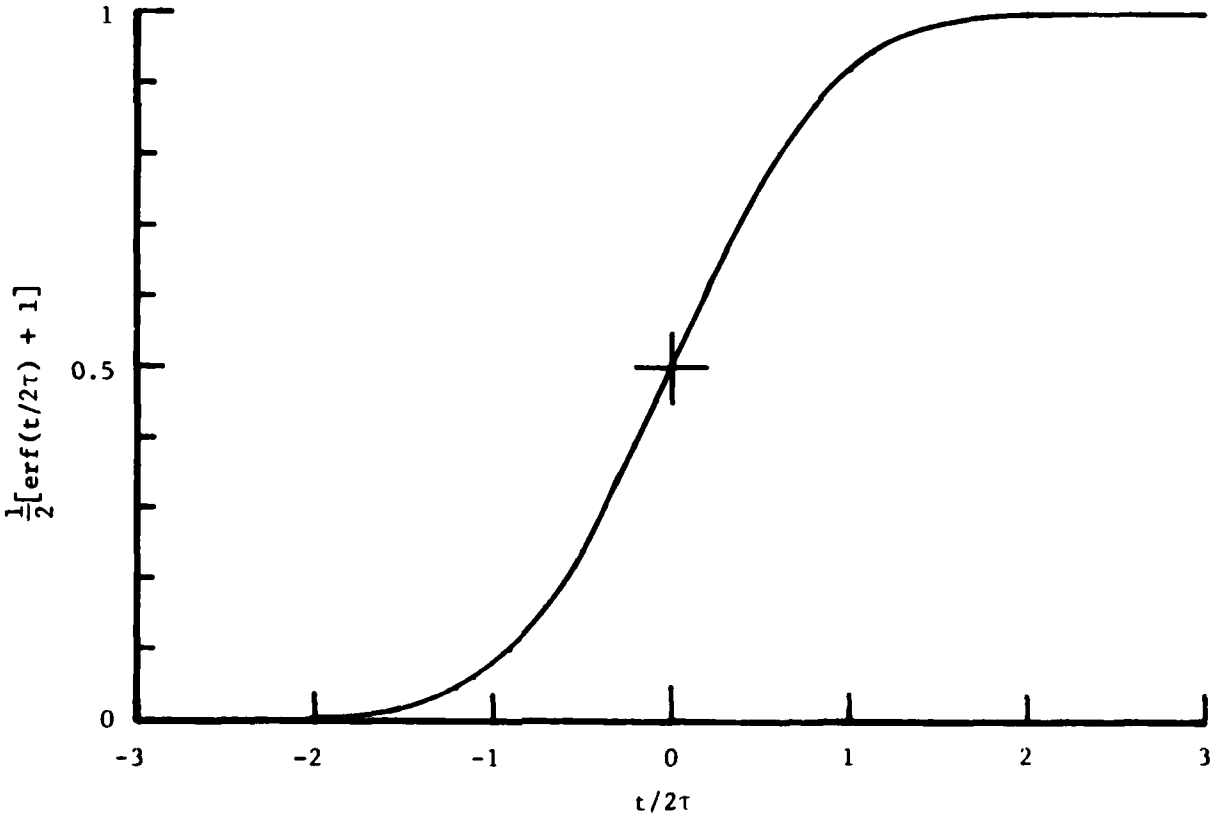

Figure 12. The shape of smoothed-out step function representing the displacement applied at the source according to (3.13).

initial result in obtaining the force-time curve from a pulse-excited piezoelectric transducer was reported[24]. When a simple method of convolution-deconvolution becomes available, it should aid greatly in determining the transfer functions of various elements in an AE systems.

III. THEORETICAL

3.1 Source Characteristics

In order to extract the information on the nature of AE sources from the detected AE signals, it is essential to develop theoretical analysis of the expected behavior of various AE sources and to predict the waveforms and/or frequency spectra of AE signals reaching a detector. A part of the analysis lies in obtaining the solution for the dynamic impulse response of a structure or simply a response function, $R(r,t)$. A few special cases have been analyzed, as discussed in the preceeding section. A typical AE source is not an impulse, but has a characteristic time dependence or a source function, $S(r,t)$. The resultant AE signal at the detector is obtained by integrating over time the product of the impulse response of the structure and the time dependence of the source; that is, taking a convolution of the response and source functions, $R(r,t) * S(r,t)$. Furthermore, when a transducer is not ideally flat in its frequency response, the impulse response of the transducers, $r(t)$, needs to be convoluted with the incident AE signals in order to determine the output of the transducer. So the AE output is given by $R(r,t)*S(r,t)*r(t)$. Thus two operations of convolution must be considered starting from the AE source function in order to predict the output of a transducer.

3.2 Theories on AE Sources

Let us first consider the theories on the AE sources. This aspect is concerned with finding the dynamic stresses or displacements produced when plastic flow or fracture occurs in an elastic medium under stress. Stresses due to the expanding crack have been treated by many investigations, including Burridge and Willis[41], Freund[42], and Stöckl and Auer[43]. A general solution was given by Burridge and Willis[41] for the expanding elliptical crack in an anisotropic solid. For a suddenly extending crack, Freund[42] determined mean normal stress $[\sigma]$ arriving at a typical point r at time $t_a = r/c_L$, where c_L is the longitudinal wave velocity. $[\sigma]$ is given by

$$[\sigma] = K_I(\pi/2r)^{1/2}\, E(x - c_F t_a, z, t_a) \qquad (3.1)$$

where K_I is the static stress intensity factor, c_F is the initial crack tip velocity and E is the angular dependent term, which is obtained numerically. Here, x is in the direction of crack propagation and z is in the direction normal to the crack plane. In the region ahead of the crack, the initial arrival is a loading wave and is a finite discontinuity in stress. The magnitude of $[\sigma]$ appears to increase roughly linearly up to c_F/c_R of 0.5, where c_R is Rayleigh wave velocity.

Stöckl and Auer[43] studied the dynamic behavior of a brittle crack

using a finite difference technique, and compared the results with experiments, which were performed with Araldite B. Here, a propagating bilaterial crack is assumed to move at a constant given velocity in an isotropic material under uniaxial tension. After travelling a certain distance, the crack stops. Displacement normal to the crack plane was found to increase linearly with time at the center of the crack, followed by a gradual decay. At other locations on the crack, time dependence of normal displacement was more complex, yet maintaining the essentially similar characteristics.

Achenbach and Harris[44] have recently studied AE signals arising from crack propagation. They employed an elastodynamic ray method for the quantitative analysis of AE due to jumps of a planar crack with a smooth edge of arbitrary shape. In this method, the amplitude of a high frequency mechanical disturbance is traced as the disturbance propagates along a ray. The analytical solution for the semi-infinite crack geometry can be obtained, from which they deduced the actual distributions of the stresses released upon the crack tip propagation. Their analysis also accounted for the curvature of the crack-edge. Two cases they considered are of our immediate interest. One of the two considers brittle fracture and the other allows yielding at a crack tip. For a crack propagating in a brittle solid, the elastodynamic crack opening displacement takes the general form of

$$u_c \propto c_F^{1/2} K_I (t - x/c_F)^{1/2} u(t - x/c_F)\, u(x) \qquad (3.2)$$

where t is time, x is the distance ahead of the crack on the crack plane and u(y) is the unit step function. The corresponding first longitudinal motion, or the radial displacement u_r at distance r from the crack tip, is given by

$$u_r \propto \left(\frac{c_F}{r}\right)^{1/2} K_I E_L(c_F,\theta)(t - r/c_T)\, u(t - r/c_L) \qquad (3.3)$$

where E_L is the term dependent on the crack velocity and the angle from the crack plane. Thus, we note a linear time dependence of u_r at the longitudinal wavefront, which implies that the particle velocity jumps discontinuously when the wavefront arrives. When a small zone of cohesive tractions at the crack tip is present, such as in the Dugdale model for plastic yielding, u_c is of the form

$$u_c \propto c_F^{1/2} K_I (t - x/c_F)^{3/2} u(t - x/c_F)\, u(x) \qquad (3.4)$$

leading to the expression for u_r of

$$u_r \propto \left(\frac{c_F}{r}\right)^{1/2} K_I E_L(c_F,\theta)(t - r/c_L)^2 u(t - r/c_L) \qquad (3.5)$$

In this case, the particle velocities are continuous at the wavefront and the AE intensity is expected to be considerably less than that for brittle fracture. The correction for curvature of the crack edge (ρ_c) enter u_r as $(1 + r/\rho_c)^{-1/2}$, indicating a decrease in AE intensity as ρ_c decreases. Other more complicated geometries were also considered.

These theories on AE due to a propagating crack predict conflicting results. This is quite understandable. Methods employed varied significantly. The initial and boundary conditions and other assumptions were not common. Still, critical evaluation of the obtained results and underlying assumption would be valuable. Comparison with well-defined experiments will be most interesting.

3.4 Theories on AE Signals

Malén and Bolin[45] developed a theory on AE signals considering a time dependent distribution of inelastic distortion $\beta^*_{ij}(r',t)$, on the basis of Mura's dynamical continuous dislocation theory[46]. Ignoring the spatial distribution of β_{ij} of the radiating source of r' and expressing the stress σ at an observation point r in terms of Fourier transformed variables, they obtained

$$\sigma_{st}(r,\omega) = -\int \mu[G_{sk,t\ell}(r,\omega) + G_{\ell k,s\ell}(r,\omega)] + \lambda\,\delta_{st}G_{qk,q\ell}(t,\omega)\}$$

$$\times \int \{\mu[\beta^*_{\ell k}(r',\omega) + \beta^*_{k\ell}(r',\omega)] + \lambda\,\delta_{k\ell}\beta^*_{nn}(r',\omega)\}\,dr'$$

$$= R_{stk\ell}(r,\omega)\,S_{k\ell}(\omega), \qquad (3.6)$$

where ω is the angular frequency, G_{ij} is the Green's function $\delta_{k\ell}$ is the Kronecker's delta, μ and λ are the Lame's constants, $R_{stk\ell}$ is the response function of the medium and $S_{k\ell}$ is the source function. Further, $G_{sk,tq} = \partial^2 G_{sk}/\partial x_t\,\partial x_q$ and summation over repeated indices is implied. The response function is basically the second derivative of the Green's function and simplified to

$$R(r,\omega) \simeq \frac{\omega^2}{4\pi r c^2}\,e^{i\omega r/c} \qquad (3.7)$$

where the orientation dependence is ignored, $c \simeq c_L \simeq c_T$ and $i^2 = -1$. It is assumed that the source function can be expressed as the product of the magnitude, S_m, and the shape function $f(\omega)$ as

$$S_{k\ell} = S_m f(\omega) = (2\mu\,\Delta\,\epsilon^*_{k\ell}V^* + \lambda\,\delta_{kk}\,\Delta\,\epsilon^*_{nn}\,V^*)\,f(\omega) \qquad (3.8)$$

where $\Delta\epsilon^*_{ij}$ is the inelastic strain increment, V* is the volume over which $\Delta\epsilon^*_{ij}$ is distributed uniformly. As usual, $\epsilon^*_{ij} = (\beta^*_{ij} + \beta^*_{ji})/2$. For a stepwise increase in $S_{k\ell}$, i.e.

$$S_{k\ell} = S_m u(t) \qquad (3.8)'$$

we obtain

$$f(\omega) = \pi\delta(\omega) - 1/i\,\omega. \qquad (3.9)$$

Malén and Bolin[45] arrived at the stress at r and t as

$$\sigma(r,t) = -\frac{\omega\Delta\omega}{4\pi^2 rc^2} S_m \sin\omega(r/c - t) \qquad (3.10)$$

where an ideal detector operates at ω with the bandwidth of $\Delta\omega$. It is assumed that ω is much smaller than the inverse of the rise time of $S_{k\ell}$. They considered three special cases of S_m; i.e., for dislocation motion, S_m is proportional to a plastic strain increment $\Delta\varepsilon^*$; for a pure dilatation, S_m varies with volume change, and for crack propagation,

$$S_m = h\sigma_a(\ell_2^2 - \ell_1^2), \qquad (3.11)$$

where h is the width of the crack that jumps from $2\ell_1$ to $2\ell_2$ under an applied stress σ_a. For the last case, it is interesting to note that, if the crack jumps only a small distance $\Delta\ell$, S_m becomes

$$S_m = 2\sigma_a \, h\cdot\Delta\ell\cdot\ell_1 \propto K_I(h\Delta\ell)\,\ell_1^{1/2}\,, \qquad (3.11)'$$

where K_I is the stress intensity factor.
This relationship has an additional square-root dependence on the crack length compared to an empirically derived expression for the magnitude of AE signal due to incremental cracking[47]. The latter was proportional to the stress intensity factor and crack area.

While reasonable estimates of the magnitude of S_m can be obtained from the above analysis, the solution in the form of (3.10) has two fundamental conflicts with observed AE behavior. Firstly, it is a continuous wave, which cannot be a response to a stepwise change in the source function. Secondly, the magnitude of stress wave increases linearly with frequency, in contrast to commonly observed trends in the opposite direction. The first difficulty is due to oversimplification in the derivation of (3.10), which will be corrected below. It can be shown that a bipolar stress pulse results from a stepwise jump in the distortion at an AE source. The second conflict is resolved also since the correct frequency spectrum of a bipolar pulse reaches a maximum, above which the power density tends to decrease with frequency.

Let us now derive the waveform without the damaging simplification employed for obtaining (3.10). The exact waveform can be obtained by taking a Fourier transform of the product of (3.7) and (3.8) with the substitution of (3.9), as follows:

$$\sigma(r,t) = \frac{S_m}{2\pi}\int_{-\infty}^{\infty} e^{-i\omega t}\,\frac{\omega^2}{4\pi rc^2}\, e^{i\omega r/c}(\pi\delta(\omega) - 1/i\omega)d\omega$$

$$= S_m\delta'(r/c - t)/8\pi^2 rc, \qquad (3.12)$$

where $\delta'(y)$ is the first derivative of the Dirac's delta function. This also corresponds to the second derivative of the unit step function, u(t). In order to examine effects of the rise time, it is more convenient to smooth out the unit step function by employing the Gauss error function.

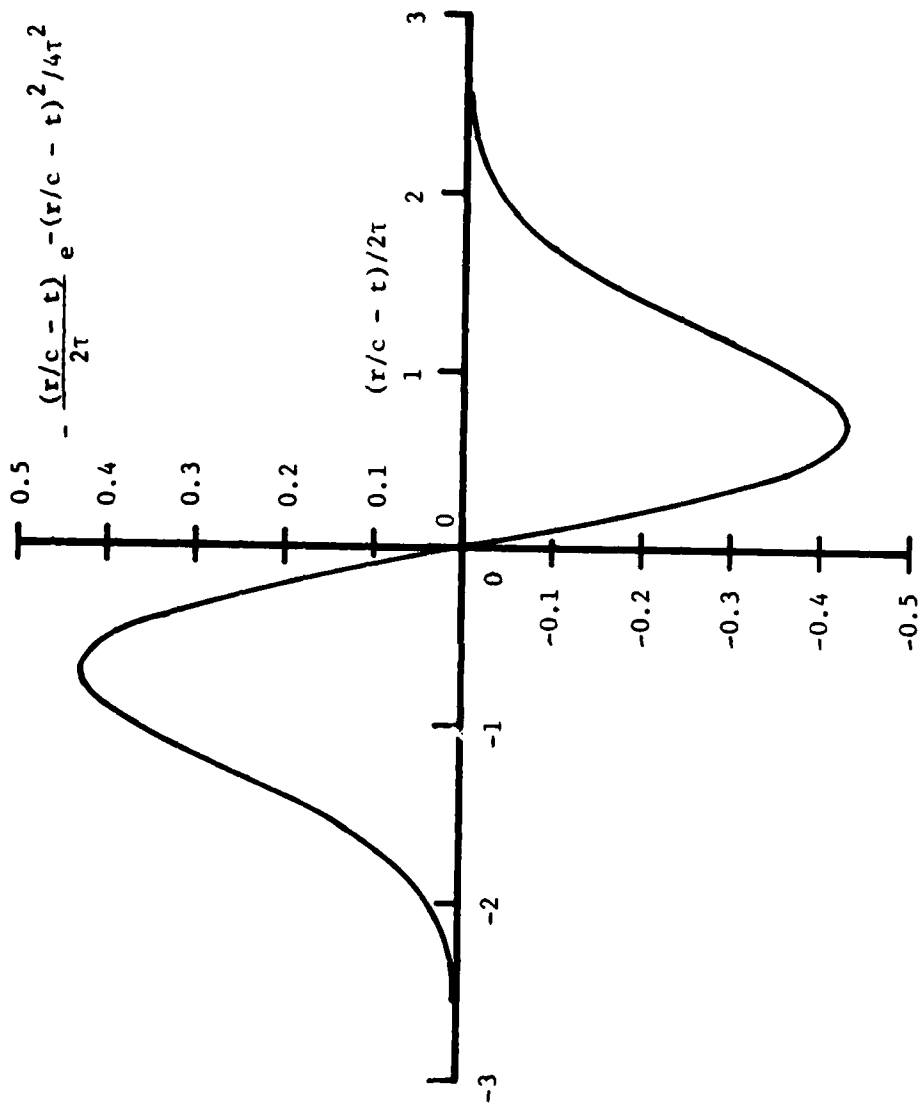

Figure 13. The shape of a bipolar stress pulse resulting from the error function displacement step (after 3,14).

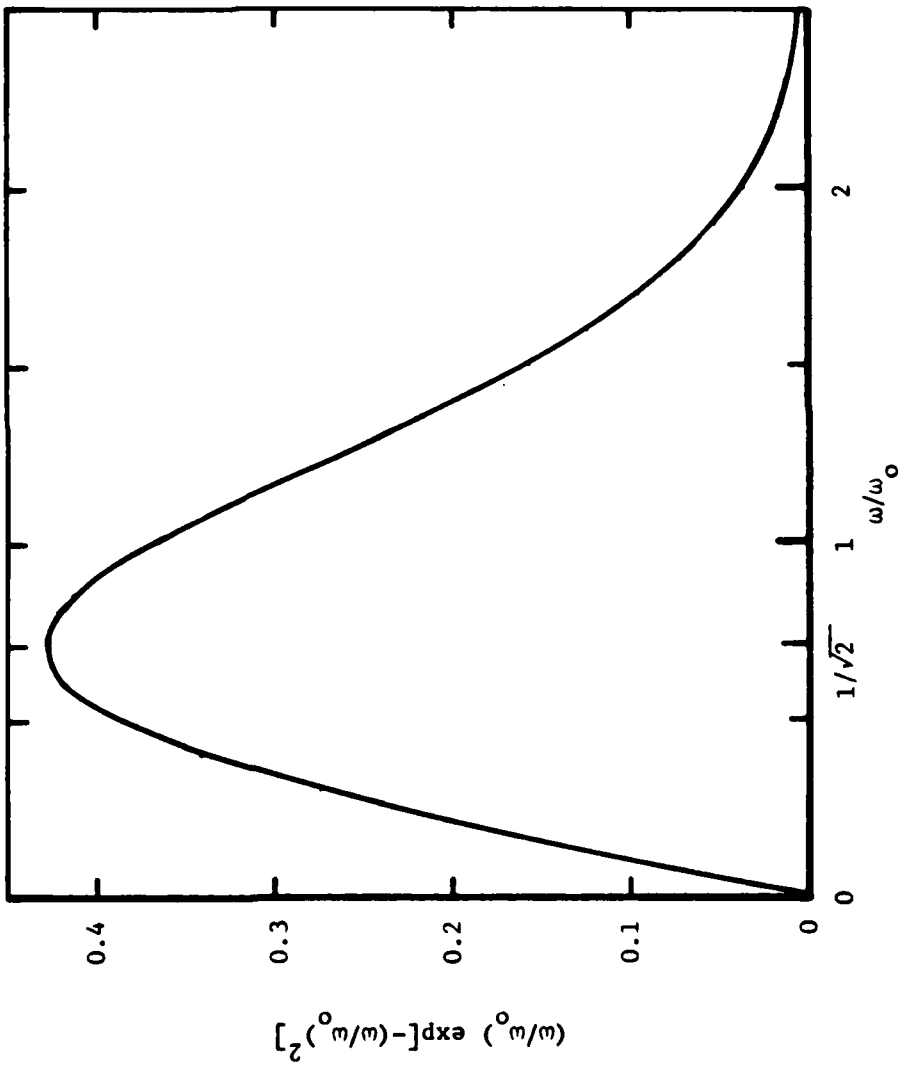

Figure 14. The frequency spectrum of the bipolar stress pulse shown in Fig. 13. The shape of this spectrum coincides with that of Rayleigh distribution function.

Following Malén and Bolin[45], we approximate u(t) by

$$u(t) \simeq \frac{1}{2}\,[\mathrm{erf}(t/2\tau) + 1]$$

$$= \frac{1}{\pi} \int_0^{t/2\tau} e^{-y^2}\, dy + \frac{1}{2}\,. \qquad (3.13)$$

The shape of this function is shown in Fig. 12. Here, the rise time, defined as time duration from 0.1 to 0.9 of the final value, is equal to 4τ. When (3.13) is assumed to represent the shape of the source function, we obtain as the stress pulse in the form of

$$\sigma(r,t) = -\frac{S_m}{8\pi^{3/2} r c^2 \tau^2}\left[\frac{(r/c - t)}{2\tau}\, e^{-(r/c - t)^2/4\tau^2}\right]. \qquad (3.14)$$

The terms in the brackets determines the shape of this stress pulse, which is illustrated in Fig. 13. The maximum and minimum in σ occur at $t = (r/c) \pm 1.41\,\tau$, and the quantity in the square brackets reaches ± 0.43. This implies that σ_{max} is proportional to $(S_m/r\tau^2)$. The frequency spectrum of (3.14) can be obtained and is given by

$$|F(\omega)| = \frac{S_m\, \omega_o}{4\pi r c^2}\, \left(\frac{\omega}{\omega_o}\right) e^{-(\omega/\omega_o)^2}\,, \qquad (3.15)$$

where $\omega_o = 1/\tau$. Figure 14 illustrated the shape of the frequency spectrum (which coincides with the shape of the Rayleigh distribution function). It is shown that the frequency response increases nearly linearly with frequency below $\omega = 0.5\omega_o$, reaches a maximum at $\omega = 0.707\ \omega_o$ and diminishes at frequencies above $\omega \simeq 2.5\ \omega_o$.

It is now easy to realize why a continuous wave solution was given as in (3.10). This is a Fourier component of the stress pulse (3.12) or (3.14), which was incorrectly represented as the stress pulse. In order to obtain the output of a narrow band transducer, which is excited by a stress pulse, it is necessary to calculate a convolution integral. This subject was discussed in detail in the paper we presented elsewhere[48]. We represented the impulse stress response of a narrow band transducer to be given by

$$r(t) = e^{-\beta t} \cdot e^{i\omega_o t} \cdot u(t) \qquad (3.16)$$

where β is a decay constant and $f_o = \omega_o/2\pi$ is the resonance frequency of the transducer. The frequency response of the transducer, F(f), is given by

$$F(f) = [2\pi i(f - f_o) + \beta]^{-1} \qquad (3.17)$$

The bandwidth (at -3dB) of the transducer is given by β/π. When the transducer is excited by a stress pulse (3.14), the transducer response $R_t(t)$ to this stimulus is given by

$$R_t(t) = \int_{-\infty}^{\infty} \sigma(\eta)\ r(t - \eta)\ d\eta. \qquad (3.18)$$

While the exact analytic integration is difficult, it can be shown that the maximum fo $R_t(t)$ is approximately proportional to the product of σ_{max} and τ and occurs at about 10τ, provided that τ is much smaller than $1/f_o$ or $1/\beta$. The decay of $R_t(t)$ is naturally dictated by the decay constant β with the oscillation centering at f_o. It is important to point out that the maximum transducer output is proportional to S_m/τ; i.e., the rise time inversely affects the transducer output. This important result is a consequence of (3.13) and (3.18).

The above results regarding the waveform and frequency spectrum of a stress pulse deduced from the Malén-Bolin analysis are quite different from the intuitive models sugggested by Stephens and Pollock[49] and by Hill and Stephens[50]. Stephens and Pollock assumed the shape of stress pulse as a Gaussian function given by

$$\sigma = \sigma_o \exp(-t^2/\tau_o^2), \qquad (3.19)$$

where τ_o define the pulse width. Its frequency spectrum is also a Gaussian function, having a maximum at $\omega = 0$ and decreasing to $1/e$ at $\omega = 2/\tau_o$. Note that (3.19) takes the form of the first derivative of (3.14), and that the first derivative of the Gaussian frequency spectrum results in the same form as (3.14). Another intuitive model suggested by Hill and Stephens[50] assumes a rectangular stress pulse with the amplitude σ_n and the width T_n. As is well known, the frequency spectrum decreases with increasing frequency having the form of $\sin(\omega T_n/2)/(\omega T_n/2)$. In both models, the frequency spectra have a maximum at zero frequency, in sharp contrast to the result of (3.15). It is interesting to note that the time derivative of (3.3), which represents the particle velocity or stress arising from the propagation of a brittle crack[44], results in a square stress pulse as proposed by Hill and Stephens[50]. This is due to the superposition of the emission from the starting event and that arising from the arrest of crack propagation after a short time, T_n. Most of the experiments discussed in the preceeding section dealt with the application of a stress step and the resultant displacement at the epicenter was essentially stepwise. This corresponds to a unipolar stress pulse, in contrast to bipolar stress pulses of (3.12) and (3.14). Some experiments also recorded unipolar and bipolar displacement pulses (see Fig. 15)[27,28]. The unipolar displacement pulses correspond to bipolar stress pulses, as expected from (3.14). The bipolar stress pulse is expected to originate from the application of a force dipole at the source[32]. Thus, it is not possible at present to single out either unipolar or bipolar pulse shapes as correct waveforms. Hopefully, future analytical studies will clarify the relationships between conditions at a source and resultant AE signals. For such efforts, it is incumbent to combine a proper Green's function and probable source functions and to account for the tensor nature of these functions.

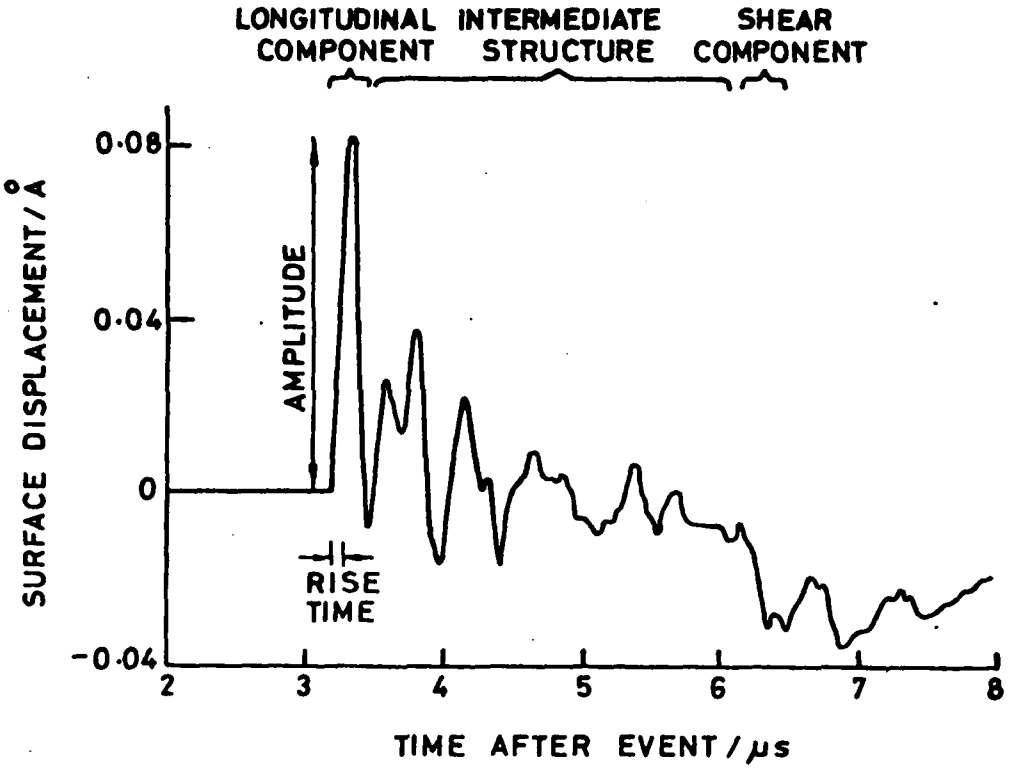

Figure 15. Three surface displacement transients measured during the ductile fracture of low-alloy steel.[28] The longitudinal leading edge (L) has variable amplitude and rise-time. There is also variation in the magnitude of the shear arrival(s) and the parts of the signal following L and S.

IV. AE BEHAVIOR OF MATERIALS

4.1 AE due to Plastic Flow

Considering AE signals generated by plastic deformation of materials, it is necessary to consider the continuous-type signals separately from the burst-type emission. The former is due to simultaneous arrival of numerous AE signals at a transducer. Because of random and high rate excitation of the transducer, waveforms are indistinguishable from random noise. This type originates mainly from the rapid motion of dislocations. The latter arises from distinct events such as twinning, decohesion or fracture of second phase particles and intergranular and transgranular cracking. In order to observe the events separately, the rate of emission must typically be less than 10,000 events per second.

In earlier models of AE due to plastic flow, distinct emission events were considered. Fisher and Lally[51] attributed an AE burst to microyielding, which manifested itself as a load drop in the stress-strain curve. Dislocation avalanche was proposed as an AE source by Agarwal et al.[52] and James and Carpenter[53]. Tetelman[54] attributed AE to the relaxation of stored strain energy within a single grain via the motion of dislocation pile-up. Gillis and Hamstad[55] considered the release of plastic work to be the source of an AE event.

On the basis of individual dislocation motion, several models have been presented. Theoretical ground work was laid by Simmons and Clough[56]. This approach parallels that of Malén and Bolin[45], and additionally considers the stochastic nature of dislocation velocity distributions. It is, however, still incomplete and makes no prediction that can be compared to experimental observations.

Phonon emission from moving dislocations was equated to AE by Kiesewetter[57] and by Rouby[58]. Kiesewetter and Schiller[57] utilized Eshelby's analysis of an acoustic Bremsstrahlung due to an accelerating (and decelerating) dislocation[59]. The radiated energy from a harmonically oscillating screw dislocation of length ℓ is given by Eshelby[59] as

$$E_h = \pi \mu b^2 \ell^2 \omega^2 \bar{v}^2 / 5c_T^3 \quad , \tag{4.1}$$

where b is the Burgers vector and $\bar{v}$ is the mean dislocation velocity. Kiesewetter and Schiller[57] assumed the product of E_h and the number of dislocation segments, n_d, to be the mean square amplitude of AE signals, $(V_r)^2$. Noting that total mobile dislocation density (ρ_d) is given by $n_d \ell$, they obtained,

$$(V_r)^2 \propto \rho_d \cdot \ell. \tag{4.2}$$

Rouby et al.[58] considered effects of grain size on the average time between the acceleration and deceleration of a moving dislocation emitted from a dislocation source at grain boundary. They assumed that such a pattern of dislocation motion produces a bipolar AE signal, from which the character-

istic spectrum was postulated. These and other attempts[60-63] to model the dislocation induced AE signals are still in a preliminary stage and even the qualitative behavior is not sufficiently clarified.

4.2 Continuous AE Signals

Let us now consider a new model based on the modified Malén-Bolin theory, presented in the preceeding section. We start with a stepwise increase in plastic strain due to dislocation motion, which produces a stress pulse at a resonant transducer. Next, the statistical nature of dislocation generation and motion is considered to predict the intensity of continuous-type AE signals.

The magnitude of plastic strain increment is S_m, as defined earlier and its time dependence follows (3.13) with a rise time of 4τ. From (3.14), the maximum in the stress pulse is proportional to S_m/τ^2, or

$$\sigma_{max} \propto S_m/\tau^2. \tag{4.3}$$

When the stress pulse excites a transducer, the peak voltage of the transducer response, R_t^{max}, is proportional to $\sigma_{max} \cdot \tau$, or

$$R_t^{max} \propto S_m/\tau, \tag{4.4}$$

according to (3.16) and (3.18). Here, we recall S_m is proportional to a plastic strain increment, $\Delta\varepsilon^*$, which is a plastic strain step produced in the material following a time function of (3.13) with the rise time 4τ. Thus, $\Delta\varepsilon^*/4\tau$ can be considered as the plastic strain rate in the localized volume and will be referred to as "instantaneous plastic strain increment", or instantaneous $\Delta\varepsilon^*$. From (4.4), the peak output of a transducer is seen to be proportional to the instantaneous $\Delta\varepsilon^*$, i.e.

$$R_t^{max} \propto \Delta\varepsilon^*/\tau. \tag{4.5}$$

During plastic deformation of a material, numerous slip steps are produced, as each distinct dislocation movement gives rise to $\Delta\varepsilon^*$. When the strain rate during a test is kept constant as in a typical tensile test, the number of events per unit time (or event rate), $\dot{N}$, is given by

$$\dot{N} = \dot{\varepsilon}/\Delta\varepsilon^*. \tag{4.6}$$

where $\dot{\varepsilon}$ is the plastic strain rate. When a large number of stress pulses arrive at a transducer from uncorrelated sources distributed throughout the sample volume, the phase of the stress pulses is randomly distributed even assuming their amplitude is given by an average value. Each stress pulse produces the peak transducer output of R_t^{max} and $\dot{N}$ events excite the transducer per unit time. This produces the root mean square transducer output V_r of

$$V_r \propto \sqrt{\dot{N}} \cdot \Delta\varepsilon^*/\tau. \tag{4.7}$$

It is important to note that V_r is not directly dependent on stress. The stress level is determined in maintaining strain rate, which is controlled by the ease of dislocation multiplication and motion.

When strain rate during a test is varied, $\Delta\varepsilon^*$ and τ are expected to remain unchanged unless the operative dislocation mechanism changes. From (4.6), $\dot{N}$ should change and V_r becomes proportional to $\sqrt{\dot{\varepsilon}}$ according to (4.7), or

$$V_r \propto \sqrt{\dot{\varepsilon}}\ \sqrt{\Delta\varepsilon^*}/\tau. \tag{4.8}$$

The square-root dependence on $\dot{\varepsilon}$ is quite commonly observed in AE due to plastic deformation[64] in agreement with the prediction of the present model.

When the number of dislocation segments increase, e.g. in cold-worked materials, one expects a proportionate reduction in $\Delta\varepsilon^*$ in a tensile test. For achieving a given strain rate, each dislocation needs to move only a small distance, when more dislocations can move. From (4.8), we find V_r to decrease as $\Delta\varepsilon^*$ becomes smaller. It can be also seen that

$$V_r \propto 1/\sqrt{\dot{N}}\ , \tag{4.9}$$

when $\dot{\varepsilon}$ and τ are unchanged. This also agrees with the generally observed situation where AE is reduced by cold-working[1,5,12].

While $\dot{\varepsilon}$, $\dot{N}$ and $\Delta\varepsilon^*$ remain constant, it is possible for τ to vary. This can happen when a dislocation breaks away from the Cottrell atmosphere, or when a dislocation encounters greater lattice friction force in a solid solution compared to a pure metal, and so on. Here, V_r varies inversely proportional to rise time, or

$$V_r \propto 1/\tau. \tag{4.10}$$

This is in accordance with expectation, although no conclusive experiment has been available to demonstrate the variation in τ.

4.3 Recent Experiments on Plastic Flow

We have studied AE bahavior of austenitic stainless steels (AISI 304L and 316) as a function of test temperature. Some of the results have been reported[65]. Since the stacking fault energy (SFE) is low in these steels, planar glide is prevalent and this is thought to be the reason why AE activities are very low[66]. At higher test temperature, SFE tends to increase and thermal activation effect also promotes non-planar glide.

In Figure 16, temperature dependence of the 0.2% offset yield strength and flow stress at 10% strain are shown together with the peak rms voltage of AE at the yielding and the AE level at 10% strain for 316 stainless steel (S. Hsu, unpublished). The results are similar to those of 304L stainless steel[65]. While the strength data showed gradual decline with temperature, AE activities exhibited dramatic increases. The peak AE level

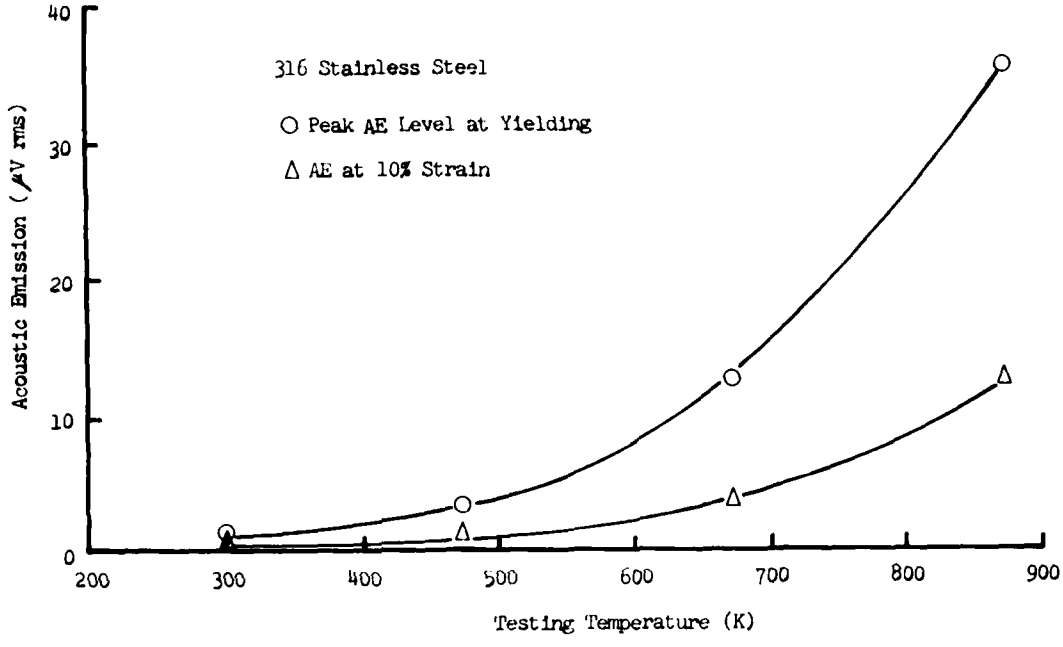

Figure 16. Temperature dependencies of the yield strength, the flow stress at 10% strain, the peak AE level at the yielding, and AE level at 10% strain for 316 austenitic stainless steel (S. Hsu, unpublished).

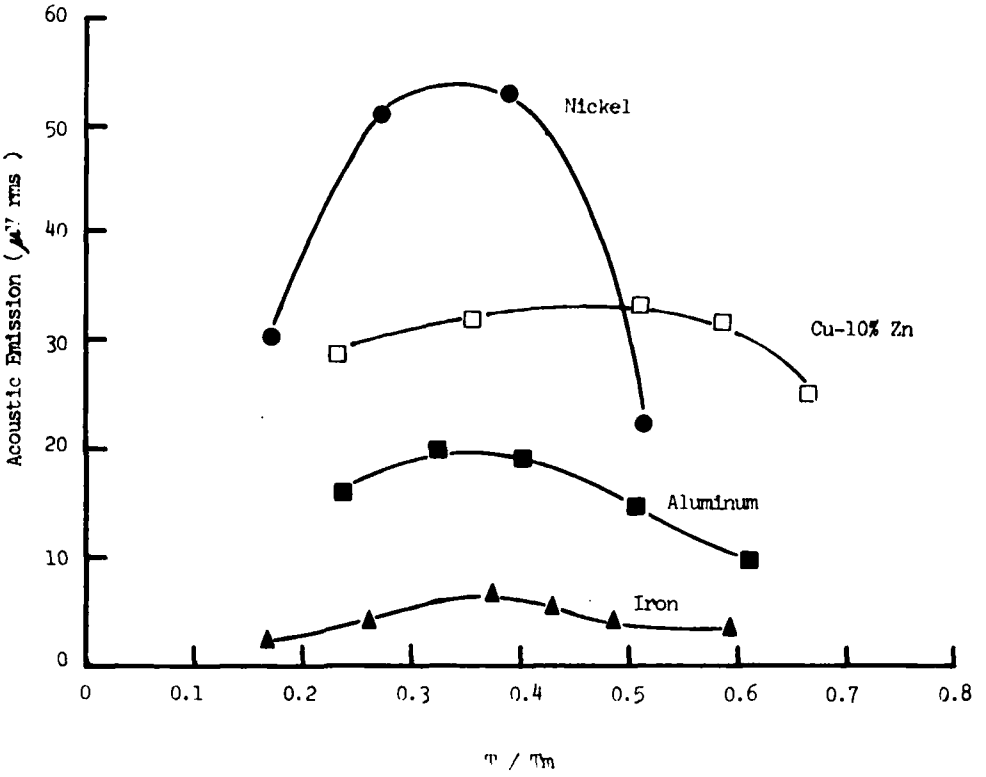

Figure 17. The peak AE level at the yielding against test temperature, normalized by absolute melting temperature for aluminum, nickel and iron (S. Hsu, unpublished).

increased ten -fold when the test temperature was raised from 300K to 873 K.

In the tests, strain rate was constant. It was also found that the AE level was dependent on the square-root of $\dot{\varepsilon}$. AE level at the yielding was unaffected by dynamic strain aging, which did not begin until some deformation had occurred. According to the model presented above, we postulate that the instantaneous $\Delta\varepsilon^*$ is smaller for the planar mode of dislocation glide than that for non-planar glide[65]. In the planar mode, a dislocation moves as a part of a pile-up and must move against the back stresses of preceeding dislocations. This limits the distance of motion and reduced the speed of dislocation motion, leading to a smaller value of instantaneous $\Delta\varepsilon^*$ and a low AE level. In the non-planar mode, tangles and cell structures are produced and each dislocation travels freely over a relatively dislocation free region between the tangles on the cell boundaries. This produces a large instantaneous $\Delta\varepsilon^*$ as well as a high AE output[65]. In both cases, the mean distance of the dislocations decreases with work hardening and AE output diminishes with plastic deformation.

Since the yield and flow stresses decrease with increasing temperature, it is obvious that plastic work[55] or strain energy relaxation[54] concepts cannot explain the observed increase in AE levels in stainless steels. It is certain that applied stress level is <u>not</u> a parameter that dierctly dictates the AE level from plastic flow. The phonon emission concept[57] cannot explain the observed temperature dependence, as (4.2) contains no temperature-related term.

Temperature dependence of AE behavior in several metals and alloys was evaluated (S.Hsu, to be published). Aluminum, nickel, iron and dilute copper-zinc alloys showed a different temperature effect, as can be seen in Figure 17. Generally, the AE level at the yielding initially increased with test temperature, then decreased after reaching a maximum. Relative changes were not as large as in stainless steels. In the materials of this group, SFE is not expected to vary significantly and glide mode remains non-planar at all temperatures.

In pure metals tested, the maximum in AE level occurred at 0.35 to 0.4 of absolute melting temperature, T_m. Below this temperature, the yield or flow stress varies strongly with temperature and the dislocation structure tends to change from more uniform distribution or loose tangles to tight tangles or well defined cell walls. In terms of the present model of AE, τ is expected to decrease with increasing temperature, resulting in higher AE levels. This is due to a higher dislocation velocity through the dislocation free zones. In this low temperature range, $\dot{N}$ and $\Delta\varepsilon^*$ are expected to change little. Above the peak temperature of 0.35~0.4 T_m, dynamic recovery and recrystallization become significant[67]. Less and less debris of dislocation motion are left within the material, requiring a lower applied stress to maintain a strain rate. Lower AE levels with increasing test temperatures can be attributed to possibly two causes. One is the reduction in the average dislocation velocity through the increase in viscous drag due to thermal activation[68]. The other is increased number of dislocations generated from the sources at grain boundaries or cell walls.

At elevated temperatures, thermal activation again is expected to ease the emission of dislocations. The two causes are interrelated, because a lower dislocation velocity requires a higher number of glide dislocations. Whichever is the primary cause, this interpretation is consistent with the decrease in the yield or flow stress with temperature.

In another study[69], we examined AE behavior of a pressure vessel steel, ASTM A533 B, which is a low carbon Mn-Ni-Mo steel. Let us consider effects of heat treatment on AE from this steel during tensile testing at room temperature. Figure 18 shows the maximum rms voltage of AE during the yielding of quenched and tempered samples as a function of tempering temperature. Samples were quenched from 930°C into water and tempered for 24 hours at each temperature. The AE level of as-quenched sample was very low, but it increased dramatically after tempering at 200 to 300°C. As the tempering temperature was raised, the peak AE level started to decline and reached a minimum at 650°C.

The as-quenched condition is a lath martensite with a very high dislocation density. Most of these dislocations are mobile, but the mean free path for each is limited because of the high density. In terms of our model of continuous AE, $\dot{N}$ is large and $\Delta\varepsilon^*$ is small. Hence, AE level is low as found in the experiment. After tempering at 300°C, rod-shaped carbides were observed in the lath martensite structure[70]. Since significant recovery is yet to occur, the dislocation density remains high. Over this range of tempering temperature, the ratio of stress at which AE becomes observable σ_{AE}, to the yield stress, σ_y, increases from 0.3 to 0.6~0.7. This implies stronger pinning of dislocations due to Cottrell atmosphere of carbon interstitials. With increasing effectiveness of dislocation pinning, the number of mobile dislocations is reduced. Another consequence of tempering is the reduction of free carbon interstitials in the matrix, resulting in the decrease of frictional stress. From these conditions, one expects dislocations unpinning during the activation of a source and a higher dislocation velocity through the tempered martensite matrix. These favor shorter rise time, larger $\Delta\varepsilon^*$ and reduced $\dot{N}$, all of which contribute to a higher AE level in moderately tempered martensite.

As tempering temperature was further increased, σ_{AE}/σ_y ratio remained high, while σ_y continued to decrease due to recovery and recrystallization of dislocation substructures. Continued carbide precipitation and coarsening are also responsible for the decrease in σ_y. After 650°C temper, fine equiaxed ferrite grains were observed via electron metallographic studies[71,72]. Large spheroidal cementite particles were found at the ferrite grain boundaries and fine dispersion of alloy carbides was observed in the grain interior. In this condition, the number of initially mobile dislocation was small and the yield point phenomenon was observed. Dislocation glide in this material is expected to originate from a few favored dislocation sources and to proceed by profuse multiplication. Thus, it is expected that $\dot{N}$ is small and $\Delta\varepsilon^*$ is large. Apparently, however, the rise time τ is large for such multiplication steps and this reduces the AE level. Actually, the observed AE level in the 650°C tempered steel is comparable to that of pure iron with a fully ferritic structure. In the latter, resi-

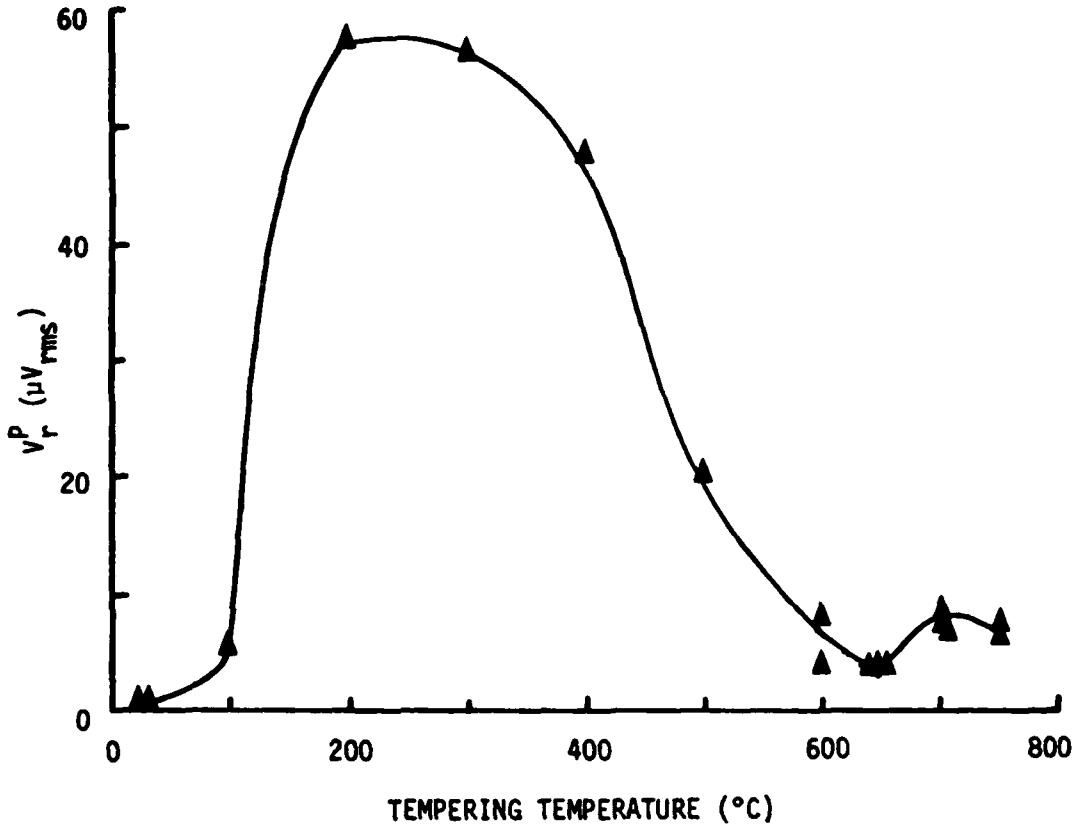

Figure 18. The maximum rms voltage (V_r^P) for martensitic A533B tensile samples as a function of tempering temperature.[69]

dual interstitial impurity atoms are expected to pin dislocation sources and similar yielding behavior is produced.

These three studies offer examples of consistent explanation of AE behavior in terms of our model of continuous-type AE signals. While further elaboration is needed on several aspects, the model can predict relative changes in AE level on the basis of dislocation dynamics. Improvements in the model and corroboration with other experimental techniques regarding independent verification on such parameters as rise time, plastic strain increment and event rate will be desirable.

4.4 AE due to Cracking

Two other articles in this Volume deal with this subject and previous studies are adequately covered there[73,74]. Here, we consider cracking induced AE in terms of the extended Malén-Bolin theory and related experimental findings.

Let us examine a thin elliptical crack of length h. The crack is subjected to normal applied stress σ_a such that Mode I crack propagation takes place. σ_a acts perpendicular to the major diameter of the crack, 2ℓ. According to Eshelby[75], normal displacement S_m is given by

$$S_m = \frac{\pi(1-\nu)}{\mu} \ell^2 h \sigma_a \tag{4.11}$$

Assuming time dependence of the displacement to be in the form of the error function (3.13), we can obtain the waveform of a stress pulse due to cracking by (3.14) by substituting (4.11). Here, the crack was thought to widen from 0 to 2ℓ under a constant stress σ_a, over a rise time of 4τ. Employing a narrow band transducer, we obtain the response of the transducer to the stress pulse by (3.16) and (3.18). The peak transducer response, R_t^{max}, is then given by

$$R_t^{max} \propto \ell^2 h \sigma_a/\tau. \tag{4.12}$$

It is noted that the peak value of AE signal due to a crack extension is proportional to applied stress and to a volumetric term $\ell^2 h$. Needless to say, the AE signal is the burst-type.

Presently, we have no direct experimental confirmation of (4.12). However, the above analysis can be used in interpreting burst-type AE, which have been observed during tensile testing of several steels[48,76,77]. From the anisotropic AE behavior with respect to the rolling direction of steel plates[76,77] and from the observed linear relationship between the sulphur content of steel and the total number of AE events[48], burst-type AE found primarily in the through-thickness samples was attributed to the decohesion of elongated MnS inclusions. This is an example of microscopic cracking. During AE tests, the cumulative distribution of AE peak amplitude was found to follow a form of the Weibull distribution[48], i.e.

$$F_e(V_p) = A \exp (- B V_p^q) \tag{4.13}$$

where F_e is the cumulative distribution, V_p is the peak voltage of a burst emission, A and B are constants. An example of such a distribution is shown in Fig. 19, where q was found to be 0.4. From a metallographic study of the same steel, the distribution of MnS inclusion size was determined. Fractional cumulative distributions $D(\ell)$ of inclusion size (ℓ) on two cross sectional planes were found to follow

$$D(\ell) = D_o \exp (- a \ell^m) \tag{4.14}$$

where D_o, a and m are constant. Values of m varied between 0.7 to 1.5, with an average of 1.2[48].

For a constant σ_a and τ, the peak AE output is governed by $\ell^2 h$ according to (4.12). Observed peak voltage V_p should be equal to R_t^{max} in this case and it follows that $V_p \propto \ell^2 h$. Size distribution of MnS inclusion was observed to differ little between the width and length. Thus, $V_p \propto \ell^3 \propto h^3$. Consequently, (4.14) can be rewritten as the distribution of peak AE amplitude V_p as

$$F_e(V_p) = A' \exp (-B' V_p^{m/3}). \tag{4.15}$$

Since $m/3 = 0.4 = q$, we find that the observed amplitude distribution function of burst AE to have an identical form as that predicted by the present theory together with the independent metallographic data. Although both theory and experiment contain numerous sources of errors, it is significant that quantitative agreement of amplitude distribution analysis is achieved.

Besides the decohesion of nonmetallic inclusions, several other microscopic fracture processes are expected to operate in the region immediately ahead of a crack-tip. These include fracture of an inclusion[78,79] discontinuous plastic flow ahead of the plastic zone[54,80], rapid coalescence of microvoids either by tearing or by shearing[47,54,80-82], cleavage and quasi-cleavage[54,81] intergranular cracking[2,26,27] and hydrogen induced cracking [54]. In many experiments dealing with these types of fracture, a power-law or an extreme value statistical law has been deduced for AE amplitude distribution[4,15,81-84]. In the case of brittle polycrystalline ceramic materials, the distribution of grain size is proposed to yield the AE amplitude distribution [15,84]. On the other hand, fracture of metallic materials has several types of microfracture events and their distribution functions are not easily measured. Some of the topics are discussed by Sano[73] and Evans[84], so we only point out the necessity of correlating AE parameters to independently measured quantities, such as the size, number and distribution of microcracks. Clear experimental confirmation of any of these mechanisms is yet to be performed. For such an endeavor, the present model of crack-induced AE should be useful.

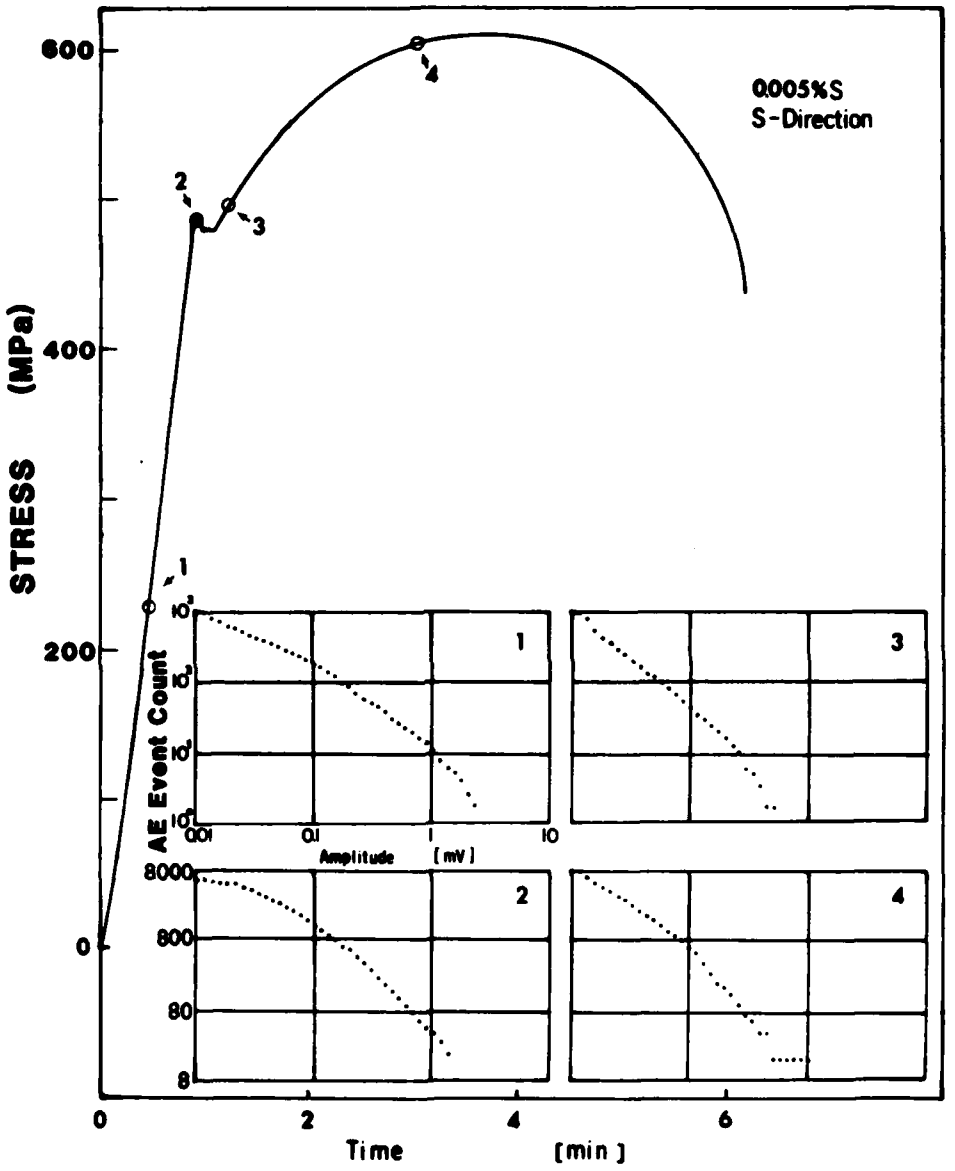

Figure 19. Stress-time curve and cumulative amplitude distribution data of burst AE during tensile testing of a thickness direction sample of as-received A533B steel. Curves 1, 2, 3 and 4 refer to stress levels of 0.5 σ_y, σ_y, 1.04σ_y and 1.25σ_y, respectively. AE event counts for 3 and 4 are 2000 counts full scale (M. Yamamoto, unpublished).

V. CONCLUDING REMARKS

Recent advances in basic studies on AE have been reviewed.

1. Toward the goal of identifying the characteristics of AE sources, significant achievements were made in developing simple AE source similators and in detecting the surface displacements via capacitive and optical transducers.

2. Elastic responses of an infinite plate to a stepwise force were theoretically clarified and experimentally verified. Other complicated force functions and finite plate sizes need to be explored to simulate a typical AE signal.

3. Determination of the transfer characteristics of a typical high sensitivity AE transducer is now feasible based on the known behavior of a simulated source and displacement transducers.

4. Real AE waveforms have been captured using a calibrated capacitance transducer and a novel specimen geometry, yobell. This should lead to a rapid expansion of our knowledge on high amplitude AE events.

5. Several theories on AE due to a propagating crack were examined. Because of varied assumptions, different results were predicted. Critical evaluation of these theoretical predictions will be required in conjunction with well defined experimentation.

6. The theory of Malén and Bolin was critically examined. Oversimplification in the original theory was deleted and correct expressions for stress pulse and frequency spectrum were derived. The maximum level of the stress pulse was proportional to the source strength and the inverse of the square of rise time.

7. Considering the transducer response, the peak transducer output due to an AE event during plastic flow was shown to depend on "instantaneous plastic strain increment". For a moving crack, the peak AE output depends on applied stress, the cube of crack size and the inverse of rise time.

8. A new model for continuous-type AE was presented. This is based on the sum of randomly arriving AE signals from instantaneous plastic strain increment. AE output depends on the square-root of strain rate, a plastic strain step and the inverse of rise time of an event, but is independent of stress.

9. Three new sets of experimental results were discussed in conjunction with the proposed model of continuous AE. It was shown that most results can be rationally interpreted.

10. A model for crack-induced AE was discussed in relation to the amplitude distribution analysis of burst-type AE in low alloy steels. The observed distribution agreed well with the predicted one based on an independent metallographic study.

This review concentrated on basic aspects of AE research and several recent studies of AE behavior of materials. It is evident that we have gained much ground in understanding the nature of AE signals and their generation mechanisms. Still, we must incorporate the advances of these studies into a wider spectrum of AE investigations and achieve better characterization of AE behavior. The goal of quantitative determination of AE parameters remains elusive. It is hoped that this review will be helpful in accomplishing this objective.

VI. ACKNOWLEDGEMENT

The author gratefully acknowledges helpful discussions and capable assistance of Drs. H. Hatano, M. Shibata, and H. Yamauchi, and Messers. S. Hsu and R. Landy, as well as the support for this research by the Office of Naval Research, Physics Program.

REFERENCES

1. P.H. Hutton and R.N. Ord, "Research Techniques in Nondestructive Testing", edited by R.S. Sharpe, Academi Press, New York, 1970, pp. 1-30.

2. "Acoustic Emission" ASTM STP 505, edited by R.G. Liptai et al., Am.Soc. Testing and Mat., Philadelphia, 1972.

3. J.C. Spanner, "Acoustic Emission, Techniques and Applications", Intex Publishing Co., Evanston, Il. 1974.

4. A.A. Pollock, Acoustic and Vibration Progress" vol. 1, edited by R.W.B. Stephens and H.G. Leventhall, Chapman and Hall, London, 1974, pp. 53-84.

5. A.E. Lord, Jr., "Physical Acoustics" vol. 11, edited by W.P. Mason and R.N. Thurston, Academic Press, New York, 1975, pp. 289-353.

6. "Monitoring Structural Integrity by Acoustic Emission", ASTM STP 571, edited by J.C. Spanner and J.W. McElroy, Am. Soc. Testing Mat., Philadlephia, 1975.

7. "The Second Acoustic Emission Symposium", Japan Indust. Planning Assoc., Tokyo, 1974.

8. "The Third Acoustic Emission Symposium", Japan Indust. Planning Assoc., Tokyo, 1976.

9. S.P. Ying, "CRL Critical Reviews in Solid State Science" 4 (1973) 85-123.

10. "Acoustic Emission" in Metals Handbook, 8th Edition, vol. 11, Nondestructive Inspection and Quality Control, Am. Soc. Metals, Metals Park, OH., 1976, pp. 234-43.

11. "Acoustic Emission/Microseismic Activity in Geologi Structures and Materials", edited by H.R. Hardy, Jr., and F.W. Leighton, Trans. Tech. Publ., Clausthal, Germany, 1977.

12. A series on Acoustic Emission, Non-destructive Testing, June 1973, 152-58, Oct. 1973, 264-69; Dec. 1973, 299-306; April 1974, 82-91; June 1974, 137-44.

13. "Acoustic Emission" edited by R.W. Nichols, Appl. Sci. Publishers, Barking, Essex, 1976.

14. "Acoustic Amission" Session 3K, Proc. 8th World Conf. on NDT Sept. 1976. Cannes, France.

15. A.G. Evans and M. Linzer, "Annual Rev. Mat. Sci." vol. 7, Annual Rev. Inc., Palo Alto, CA. 1977, pp. 179-208.

16. L. Knopoff, J. Appl. Phys. 29 (1958) 661-70.

17. F.R. Breckenridge, C.E. Tschiegg and M. Greenspan, J. Acoust. Soc. Am. 57 (1975) 626-31.

18. K. Ono and H. Icisik, Mat. Eval.33 (1975) 32-44.

19. L.J. Gr-ham and G.A. Alers, Mat. Eval. 32 (1974) 31-37.

20. L.J. Graham and G.A. Alers, Ref. 6, pp. 11-39.

21. E.G. Henneke, II, and H.W. Herring, "Composite Reliability", ASTM STP 550, Am. Soc. Testing and Mat., Philadelphia, 1975, pp. 202-14.

22. A.G. Evans, H. Nadler, and K. Ono, Mat. Sci. Engr. 22 (1976) 7.

23. W.F. Hartman and R.A. Kline, Mat. Eval. 35 (1977) 47-51.

24. N.N. Nsu, J.A. Simmons and S.C. Hardy, Mat. Eval. 35 (1977) 100-6.

25. M.A. Hamstad and R.G. Patterson, "Composite in Press. Vessels and Piping" ed. by S.V. Kulkarni and C.H. Zweben, Am. Soc. Mech. Eng., New York, 1977, pp. 141-63.

26. H.N.G. Wadley and C.B. Scruby, Acta Met. (in press).

27. C.B. Scruby and H.N.G. Wadley, J. Phys. D. (in press).

28. C.B. Scruby, J.C. Collingwood and H.N.G. Wadley, J. Phys.D.(in press).

29. C.L. Pekeris, Proc. Nat. Acad. Sci., 41 (1955) 469-80.

30. C.L. Pekeris and H. Lifson, J. Acoust. Soc. Am., 29 (1957) 1233-38.

31. W.J. Pardee, J. Math. Phys. 18 (1977) 676-86.

32. A.N. Ceranoglu and Y. H. Pao, (to be published).

33. S.L. McBride and T.S. Hutchison, Can. J. Phys. 54 (1976) 1824-30.

34. H. Hatano and E. Mori, J. Acoust. Soc. Am. 58 (1976) 344-49.

35. H. Hatano, (to be published).

36. A.E. Wehrmeister, Mat. Eval. 35 (1977) 45-47.

37. B.W. Maxfield and J.K. Hulbert, "Proc. 10th Symp. on Nondestructive Evaluation" Southwest Res. Inst., San Antonio, Texas, 1975, pp. 44-62.

38. C.H. Palmer and R.E. Green, Mat. Eval. 35 (1977) 107-12.

39. J.D. Blacic and R.L. Hagmann, Rev. Sci. Instrum. 48 (1977) 729-32.

40. J.R. Houghton and P.F. Packman, "Proc. 8th World Conf. on NDT", Paper 3K2, Cannes, France, 1976.

41. R. Burridge and J.R. Willis, Proc. Camb. Phil. Soc. 66 (1969) 443-68.

42. L.B. Freund, J. Appl. Mech. 39 (1972) 601-2.

43. H. Stockl and F. Auer, Int. J. Fracture, 12 (1976) 345-58.

44. J.D. Achenbach and J.G. Harris (to be published).

45. K. Malen and L. Bolin, Phys. Sol. (b) 61 (1974) 637-45.

46. T. Mura, "Adv. in Mat. Res." ed. H. Herman, vol.3, Wiley, New York. 1968, pp. 1-108.

47. J.D. Desai and W.W. Gerberich, Engr. Fracture Mech. 7 (1975) 153-65.

48. K. Ono, R. Landy and C. Ouchi, "The 4th AE Symposium" Int. Tech. Exchange Center, Tokyo, 1978, pp. 433-45.

49. R.W.B. Stephens and A.A. Pollock, J. Acoust. Soc.Am., 50 (1971) 904-10.

50. R. Hill and R.W.B. Stephens, Acoustica, 31 (1974) 224.

51. R.M. Fisher and J.S. Lally, Can. J. Phys. 45 (1967) 1145-59.

52. A.B.L. Agarwal, J.R. Fredrick and D.K. Felbeck, Met. Trans. 1 (1970) 1069-71.

53. D.R. James and S.H. Carpenter, J. Appl. Phys. 42 (1971) 4685-97.

54. A.S. Tetelman, UCLA-ENG-7249, July 1972.

55. P.P. Gillis and M.A. Hamstad, Mat. Sci. Engr. 14 (1974) 103-8.

56. J.A. Simmons and R.O. Clough, "Proc. 8th World Conf. on NDT" Paper 3K1, Cannes, France, 1976.

57. N. Kiesewetter and P Schiller, Phys. Stat. Sol. A38 (1976) 569-76.

58. D. Rouby, P. Fleischmann, and P.F. Gobin, "Internal Friction and Ultrasonic Attneuation in Solids", ed. by R.R. Hasiguti and N. Mikoshiba, Univ. Tokyo Press, Tokyo, 1977, pp. 311-15.

59. J.D. Eshelby, Proc. Roy. Soc., 260 (1962) 222.

60. H.L. Dunegan and D.O. Harris, Ultrasonics, 7 (1969) 160-69.

61. V.D. Natsik and K.A. Chishko, Sov. Phys. Sol. State, 14 (1973) 2678-82.

62. B. Cortellazzi et al., J. Appl. Phys. 44 (1973) 1518-23.

63. K. Kuribayashi and T. Kishi, Mat. Sci. Engr. 33 (1978) 159-63.

64. T. Kishi and K. Kuribayashi, this Volume.

65. S. S.-Y. Hsu, K. Ono and H. Hatano, Mat.Sci. Engr.38 (1979) 187.

66. H. Hatano, J. Appl. Phys. 48 (1977) 4397.

67. H.J. Mc Queen, Met. Trans. 8A (1977) 807-824.

68. W.P. Mason, "Dislocation Dynamics", ed. A.R. Rosenfield et al., McGraw Hills, New York, 1968, pp. 487-505.

69. R. Landy, M.S. Thesis, University of California, Los Angeles, Calif. March 1979; also ONR Tech. Report No. 79-02, Univ. of Calif. May 1979 (AD A069965).

70. G.R. Speich, Trans. TMS-AIME, 245 (1969) 2553.

71. K.J. Irvine and F.B. Pickering, J.I.S.I., 194 (1960) 137.

72. T. Enami et al., Kawasaki Steel Tech. Report, 6 (1974) 15.

73. K.Sano and K. Fujimoto, this Volume.

74. A.G. Evans, this Volume.

75. J.D. Eshelby, "Progress in Solid Mechanics", vol. 2, North Holland, Amsterdam, 1961, pp. 89-140.

76. K. Ono, G. Huang and H. Hatano, "Proc. 8th World Conf. on NDT", Cannes, France, paper 3K3, 1976.

77. K. Ono, G. Huang and A. Kawamoto, "Internal Friction and Ultrasonic Attenuation in Solids" Univ., Tokyo Press, Tokyo, Japan, 1977, pp. 829-34.

78. M.A. Hamstad, R. Bianchetti and A.K. Mukherjee, Engr. Fracture Mech., 9 (1977) 663-674.

79. H. Hatano and K. Ono, "The Third AE Symposium", Japan Ind. Plann. Assoc., Tokyo, 1976, pp. 475-91.

80. I.G. Palmer and P.T. Heald, Mat. Sci. Engr. 11 (1973) 181.

81. Y. Nakamura, C.L. Veach and B.O. McCauley, Ref. 2, pp. 164-86.

82. G.Clark and J.F. Knott, J. Metals Sci. 11 (1977) 531.

83. K. Mogi. Bull. Earthquake Res. Inst. (Univ. of Tokyo), 40 (1962) 831-53.

84. A.G. Evans and L.J. Graham, Acta Met. 23 1303-12.